The Use of a Novel Residuum Model to Design a Variable-Impedance Transtibial Prosthetic Socket

by

David Moinina Sengeh

B.A., Harvard College (2010)
M.S., MIT (2012)

Submitted to the Program in Media Arts and Sciences,
School of Architecture and Planning,
in partial fulfillment of the requirements for the degree of

Doctor of Philosophy in Media Arts and Sciences
at the
MASSACHUSETTS INSTITUTE OF TECHNOLOGY

February 2016

Signature redacted

Author _____
David Moinina Sengeh
Program in Media Arts and Sciences
January 8, 2016

Signature redacted

Certified by ___
Hugh Herr
Associate Professor of Media Arts and Sciences
Program in Media Arts and Sciences
Thesis Supervisor

Signature redacted

Accepted by _____
Pattie Maes
Academic Head
Program in Media Arts and Sciences

The Use of a Novel Residuum Model to Design a Variable-Impedance Transtibial Prosthetic Socket

by

David Moinina Sengeh

Submitted to the Program in Media Arts and Sciences,
on January 8, 2016 in partial fulfillment of the requirements for the degree of
Doctor of Philosophy in Media Arts and Sciences

ABSTRACT

For people living with limb amputation, the prosthetic socket – the interface between the residuum and prosthesis – is the most critical component. When a socket is uncomfortable, especially due to poor fit, the quality of life for a patient is greatly hindered. However, conventional design of sockets is largely artisan, with limited input of quantitative data. Current computer-aided and manufacturing (CAD/CAM) designs are still not clinically applicable solutions. Due to model identification procedures that employ non patient-specific and incomplete data sets, today's finite element (FE) models of the residuum are not predictive, leading to suboptimal socket designs. As such, there exists a need for a comprehensive biomechanical model of the residuum for the quantitative design and computational evaluation of patient-specific prosthetic sockets. This thesis presents a combined experimental-numerical approach to evaluate and validate a transtibial residuum biomechanical model. The central hypothesis of the work is that a single biomechanical model can predict the large non-linear response at various sites on a residuum under load. To evaluate this hypothesis, a non-linear, two-tissue model was formulated where tissue geometries were defined using MRI data of the residuum. The non-linear viscoelastic material parameters of the model were identified through inverse FEA-based optimization using *in-vivo* indentation experimental data at four locations. Using optimized model tissue parameters, the mean percentage error (mean absolute error/ maximum experimental force) between the experimental and simulation force-time curves at 14 other locations across the evaluated transtibial residuum was $7 \pm 3\%$. Using this same modeling methodology and a single set of material constants to describe the bulk soft tissue biomechanical response of seven distinct transtibial residual limb models, the average percentage error for indentations at multiple locations across all seven limbs was $7 \pm 1\%$. From these predictive models of residuum limbs, one rigid novel socket and two multi-material transtibial sockets were designed, fabricated and evaluated through an entirely quantitative, automated and repeatable methodology. In a preliminary clinical investigation, the novel sockets were shown to reduce peak contact pressures at the tibia and fibular head regions on the residuum by significant amounts during standing compared to a conventional socket interface designed and fabricated by a trained prosthetist.

Thesis Supervisor: Hugh M. Herr
Title: Associate Professor of Media Arts and Sciences

The Use of a Novel Residuum Model to Design A Variable-Impedance Transtibial Prosthetic Socket

by

David Moinina Sengeh

The following people served as members of the dissertation committee:

Signature redacted

Thesis Supervisor_____

Hugh Herr
Associate Professor of Media Arts and Sciences
MIT, Cambridge

Signature redacted

Thesis Reader _____

Neri Oxman
Associate Professor of Media Arts and Sciences
MIT, Cambridge

Signature redacted

Thesis Reader _____

Nicholas Negroponte
Professor of Media Arts and Sciences
MIT, Cambridge

Signature redacted

Thesis Reader _____

Dr. Kevin Moerman
Postdoctoral Associate, Program in Media Arts and Sciences
MIT, Cambridge

Acknowledgements

Many people have offered me countless resources and immeasurable time in my academic endeavor and for that I am forever grateful. Undoubtedly, I will not be able to thank each and every one of you via this document but do know that you are in my heart. Thank you!

That said, I would like to especially thank a few people in this document. Without Steven Shannon, Atsushi Takahashi and members of the Martinos Imaging Center at MIT, there would have been no imaging research data to start with.

Thanks to Bob Emerson who – as a friend, mentor, advisor, and prosthetist extraordinaire – made this work better through his questions and feedback and by directly building sockets, molds, liners and everything else we have needed to test our hypotheses.

The Biomechatronics Group has been my home these past six years and it still feels like I just started yesterday. Sarah Hunter, Lindsey Reynolds and all Biomechers made this possible. All the graduate students, post docs, research scientists, and undergraduates in the lab over this period have been amazing. Special thanks go to current colleagues David Hill, Luke Mooney, Madeleine Abromowitz, and Michael Eilenberg. All my UROPs over these years were amazing independent leaders, with a special mention of Daivon Dean, who has worked with me the last two years on most aspects of the research.

My two primary collaborators deserve special recognition. Kevin Moerman taught me (almost) everything I know about soft tissue modeling. He also made available his open source toolbox GIBBON Code, which was heavily used in this work. Arthur Petron designed the FitSocket system, which was used to acquire the experimental data to inform my models.

I want to express my sincere gratitude to my adviser, Hugh Herr aka "the Hughman," and the "Boss," for giving me a platform to ask questions and get this work done. Thank you to my committee members: Nicholas Negroponte, Kevin Moerman, and Neri Oxman.

Thank you to Nicholas Negroponte and Debbie Porter for introducing to the Media Lab in the first place and for the continued support as my mentors, friends, and advisers.

The MIT Media Lab community under the leadership of Frank Moss and Joi Ito will always be home to me. Thanks to Linda Peterson, Keira Horowitz, Monica Orta and all of the MAS staff for making the lab welcoming and supportive.

Thank you to my family. It has been 11 years since I left home for "school." Thanks for your support and patience.

To my dear wife Kate Krontiris: well, I am a better person because of you!

Dedicated to ***NiSo***

Table of Contents

Chapter 1

1. Introduction

The number of people living with limb loss is expected to double by 2050, from an estimated 1.6 million in 2005 (1). The majority of patients living with amputations, and in particular those with lower-limb amputations, are unsatisfied with their prosthetic socket (2). The socket remains an important product in their lives, yet its design and manufacture is still largely artisanal. As such, the socket production process is non-standard non-repeatable and its performance varies between manufacturers (3)(4). Therefore, many patients experience discomfort with their sockets due to improper fit, resulting in skin problems (5), pressure sores, and deep tissue injury (6). When a socket is uncomfortable, it limits the ability of the amputee to participate freely in daily activities, including standing and walking. The high pressures exerted upon the residual limb from a prosthetic socket can often lead to soft tissue damage (7).

These damages and large internal tissue stresses and strains caused by the loading conditions associated with particular socket designs can be evaluated using computational modeling (8). When combined with advanced computer-aided design and manufacturing (CAD/CAM) techniques, computational modeling is a powerful tool for novel socket designs. Lee and Zhang (2007), for example, presented a computational methodology for using pressure and pain evaluated on a residuum model to design better fitting sockets. While such a framework could enable prosthetists to design sockets in a more data-driven and repeatable manner, the authors assumed that the mechanical response of the soft tissue was linearly elastic with constants obtained from literature (9). However, to enable computational socket design methodologies, finite element models of the residuum should be used to accurately describe the patient-specific geometry, as well as the non-linear elastic and viscoelastic behavior of the underlying soft tissues.

Today, prosthetic socket design is not optimal, whether using conventional methodologies or CAD/CAM processes (10)(11). As such, there are reported discrepancies in the quality of sockets produced by prosthetists including those that are manufactured at central fabrication centers (3). Since conventional socket design hinges on the experience of the prosthetist and direct feedback from the amputee, the set of quantitative information recorded during the design and fabrication processes and the manner in which that information is used is limited, incomplete and varied. To advance the field, there thus needs to be a process that integrates patient-specific biomechanical modeling, design, and fabrication in a continuously quantitative and repeatable manner.

Advances in medical imaging, biomechanical modeling, and computer-aided manufacturing present new tools for such a design of prosthetic sockets. Magnetic resonance imaging (MRI) data provide accurate representation of both the outer surface and the internal 3-D geometry used to develop residuum models (12). The characteristic residuum tissue behaviors can be accurately studied using inverse finite element analyses (FEA) (13)(14). Experimental-numerical approaches are used to identify the patient-specific material constants of the residuum models at large displacements. Given these observed advances in tools and processes that can be used for prosthetic socket design, there is still no functional CAD/CAM prosthetic socket whose entire spatial material properties and final shape is truly patient- and load-specific – and dependent on an accurate and validated biomechanical residuum model. State-of-the-art reviews show current standards are not in clinical use (15) (16). This thesis aims to investigate the design of such a socket using purely quantifiable data in a repeatable and optimized process. Through a combination of FEA and rapid prototyping, novel socket designs whose shape and material properties are quantitatively determined could be manufactured, evaluated and clinically tested.

1.1. Research Statement and Hypothesis

This research project broadly contributes to the science and design of patient-specific mechanical wearable devices for the human body. More specifically, this thesis informs the design principles for a transtibial prosthetic socket, using digital anatomical models with validated material parameters.

1.1.1. Hypothesis 1

Using a combined experimental-numerical approach, a single FEA model of a transtibial residuum with a single optimized constitutive material parameter set can describe the non-linear elastic and viscoelastic tissue behavior for indentations across multiple sites on a residual limb.

1.1.2. Hypothesis 2

A single constitutive law and material parameter set can describe the non-linear elastic and viscoelastic biomechanical tissue response at various indentation sites across the residual limb of multiple patients (N=7 residual limbs).

1.1.3. Hypothesis 3

Using a validated patient-specific biomechanical model of a transtibial residuum, a multi-material prosthetic socket can be designed such that its equilibrium shape and spatial material property at each surface element area are optimized to lower socket contact pressure on the residuum, particularly at bony regions.

1.2. Thesis Outline

There were three studies conducted to directly investigate and evaluate the

hypotheses of this thesis. The findings from these studies were written for publication at appropriate journals in the fields of soft tissue modeling and prosthetic socket design. These studies make up the thesis, as outlined below:

- **Chapter 2** (Study I): Development and evaluation of a framework that describes a predictive biomechanical model of a transtibial residuum through an experimental-numerical optimization approach.
    - Development of FE model of a transtibial residuum from MRI. The surface geometry of the model consists of a skin-adipose layer in series with an internal muscle-soft tissue layer that is attached to the internal bones.
    - Use of inverse FEA (iFEA) to identify the appropriate constitutive material law that captures the large non-linear, viscoelastic soft tissue deflections using *in-vivo* indentation at various sites (N=4).
    - Evaluation of model predictability (i.e., the mean percentage error between the experimental and simulation force-time curves) across multiple indentation sites (N=14) of the residuum.

- **Chapter 3** (Study II): Investigation of soft tissue material parameter variation among multiple transtibial residuum models (N=7).
    - Use of iFEA to accurately model and characterize constitutive parameters for N=7 transtibial residual limb models.
    - Investigation of the differences in model predictability for a general set of material constants versus those from a patient-specific material optimization.

- **Chapter 4** (Study III): A preliminary clinical evaluation of novel socket designs whose shape and material mechanical impedance were defined entirely through a quantitative process.
    - Interface shape: Determination of a pressure field applied to a biomechanical model of a residuum FE model to define equilibrium socket shape.
    - Interface material: Definition of a spatially varying socket where each material surface area element is chosen to lower the surface pressure on the residuum during full body weight standing.

- **Chapter 5** (Summary and general discussions): Summary of results from the three studies presented in this thesis, with a discussion of the limitations, and future work.

2. Chapter 2: Study I

Multi-Material 3-D Viscoelastic Model of a Transtibial Residuum from *In-vivo* Indentation and MRI Data

*David M. Sengeh, Kevin M. Moerman, Arthur Petron, Hugh Herr**

Center for Extreme Bionics, Massachusetts Institute of Technology, Cambridge, MA, USA

Abstract

The socket is a critical component in a prosthetic system for a person with limb amputation. However, the methods of its design are largely artisanal. A major roadblock for a repeatable and quantitative socket design process is the lack of predictive and patient specific biomechanical models of the residuum. This study presents the evaluation of such a model using a combined experimental-numerical approach. The model geometry and tissue boundaries are derived from magnetic resonance imaging (MRI). The soft tissue non-linear elastic and viscoelastic mechanical behavior was evaluated using inverse finite element analysis (FEA) of *in-vivo* indentation experiments. A custom designed robotic *in-vivo* indentation system capable of loading the residuum at controlled rates was used to provide a rich experimental data set of force versus time at 18 sites across the limb. During FEA, the tissues were represented by two layers, namely the skin-adipose layer and an underlying muscle-soft tissue complex. The non-linear elastic behavior was modeled using 2nd order Ogden hyperelastic formulations, and viscoelasticity was modeled using the quasi-linear theory of viscoelasticity. To determine the material parameters for each tissue, an inverse FEA based optimization routine is used that minimizes the difference (combined mean of the squared force differences) between the numerical and experimental force-time curves for indentations at 4 distinct anatomical regions on the residuum. The optimization provided the following material parameters for the skin-adipose layer:
$[c = 5.22\ \text{kPa} \quad m = 4.79 \quad \gamma = 3.57\ \text{MPa} \quad \tau = 0.32\text{s}]$ and for the muscle-soft tissue complex $[c = 5.20\ \text{kPa} \quad m = 4.78 \quad \gamma = 3.47\ \text{MPa} \quad \tau = 0.34\text{s}]$. These parameters were then further evaluated to predict the force-time curves for the remaining 14 anatomical locations. The mean percentage error (mean absolute error/ maximum experimental force) for these predictions was $7 \pm 3\%$. The mean percentage error at the 4 sites used for the optimization was 4%. The predictive and patient-specific model of the residuum presented, featuring material parameters evaluated based on in-vivo indentation, may prove critical to the future advancement of quantitative methodologies for prosthetic socket design.

Key words: Transtibial residual limb, soft tissue viscoelastic properties, inverse finite element analysis

*Corresponding author address: MIT Media Lab, 75 Amherst Street, Cambridge, MA 02139, USA

2.1. INTRODUCTION

This study focuses on the use of patient-specific *in-vivo* indentation and magnetic resonance imaging (MRI) combined with inverse finite element analysis (FEA) to determine the non-linear elastic and viscoelastic mechanical properties of an individual patient's residual limb. Such a FEA model is a stepping-stone towards quantitative socket design, as it would allow for the evaluation of loading conditions such as interface pressures and internal tissue stresses and strains. The residuum is, however, a complex multi-material structure consisting of the following main tissue types: skin, adipose, skeletal muscle, tendon and bone. Portnoy *et al.* (2009) concluded that patient-specific analyses of residuum were important for evaluation of potential deep tissue injury from prosthetic devices (17). Furthermore, the soft tissues undergo large non-linear deformations and are potentially subjected to high internal strains during prosthetic socket loading (8)(18). Therefore, in order to ensure the fidelity of a residuum computational model, multiple tissue regions need to be represented in the model and the material behavior should capture the non-linear elastic and viscoelastic nature of the materials.

Previous soft tissue modeling research has been largely informed by animal tissue studies. Bosboom *et al.* (2001) presented an incompressible viscoelastic second-order Ogden model that described skeletal muscle deformation. The elastic and viscoelastic properties were identified using a numerical-experimental procedure through invasive *in-vivo* compression tests on rat tibialis anterior muscles (19). Van Loocke *et al.* (2008) performed compressive testing on porcine skeletal muscle samples demonstrating the anisotropic, non-linear elastic and non-linear viscoelastic behavior of skeletal muscle tissue (20,21). The non-linear elastic and viscoelastic behavior were modeled using an extension of Hooke's law with strain-dependent Young's moduli, and a Prony series expansion, respectively. However the elastic formulation used cannot easily be incorporated for computational modeling, and the parameters employed do not respect the constraints imposed by Hooke's law for transverse isotropy. To study soft tissue viscoelastic stress and shear response, Palevski *et al.* (2006) conducted a detailed study on porcine gluteus *in-vitro* and assumed muscle to be isotropic and linear elastic (22). Although these animal studies offer an insight into the mechanical behavior of soft tissue, the results obtained cannot easily be translated to human applications let alone use for the residuum and socket design optimization.

The mechanical behavior of human tissues have been modeled and evaluated by other researchers. For example, to inform better micro needle designs, Groves *et al.* (2012) modeled a multilayer skin using 1st order Ogden material coefficients and evaluated it by using *in-vivo* indention experimental data (23). Tran *et al.* (2007) used MRI and indentation to study the mechanical properties of human skin and muscle tissue modeled as a multi-layered neo-Hookean material (24). The indentations in both studies were on the arm: the former applying small forces in comparison to loads on the residuum, while the latter used a two-dimensional model for analyses. Dubuis *et al.* (2011) used a mixed numerical-experimental method to study patient-specific soft tissue behavior of the lower limb through FEA compressive sock induced loading (25). In that study, the adipose and skeletal

muscle tissues were jointly modeled as a neo-Hookean material. The authors concluded that segmenting specific layers of the anatomy were useful for FEA approaches in order to understand internal tissue response.

While others have further used indenters to measure viscoelastic responses over various anatomical locations on human limbs, the conclusion was that the biomechanical material constants could not be readily extrapolated to other anatomical sites on the same residuum, or across separate residuum. Tönük and Silver-Thorn (2003) presented multiple reasons for the variability and lack of model predictability across the residuum. Their model simulations failed to converge at large deformations (>75% soft tissue thickness) and at thin but stiff regions (14). Vannah and Childress (1996) also concluded that it was not possible to accurately and consistently model the biomechanical response of a bulk soft tissue across various locations on a limb using the same material constants (26). Location dependent material constants make it difficult to integrate these models into quantitative socket design and other soft tissue modeling applications.

Recent work in residuum soft tissue modeling include studies describing the impact of socket design on internal soft tissues of the residuum (8,27), and those focused on the surface pressures (28,29) and stresses at the socket-residuum interface (18). To evaluate internal soft tissue deformation in the muscle flap of the residual limb during static loading within a socket, Portnoy *et al.* (2008) used a computational model composed of two materials, the skin, and an internal soft tissue attached to rigid bones (8). A neo-Hookean strain energy function described the instantaneous stress response of the muscle tissue coupled with a Prony Series expansion to capture viscoelasticity. The skin was modeled with a James-Green-Simpson strain energy function using material constants from literature (Hendriks *et al.* (2003) (30)). The residuum model was evaluated by comparing peak pressures measured with sensors within a custom cast/socket with those predicted by the combined residuum-cast model after the boundary conditions were applied. The peak pressures varied within 10 kPa between the experimental and simulation data. With all constitutive soft tissue material parameters obtained from literature rather than from patient-specific investigations, the authors limited their study by a lack of appropriate constitutive data. However, the conclusions about inhomogeneous internal compressive stress and strain distributions from that research especially around bony areas could be used to inform the design of quantitative prosthetic interfaces and further motivates the goal of developing predictive patient-specific validated residuum models.

The objective of this study is thus to advance a patient-specific, multi-material 3-D model of a transtibial residuum for a single patient, which would allow for the evaluation of loading conditions on the residuum from a prosthetic socket. We hypothesize that a FEA model composed of two layers of homogeneous materials (i.e. constant properties across the limb) can describe the non-linear elastic and viscoelastic tissue behavior for indentations across the limb. To evaluate this hypothesis, we used a combined experimental-numerical approach. A 3-D FEA model of a residual limb was created based on segmentation of detailed MRI data. Two tissue material were specifically modeled, a skin-adipose layer and an internal muscle-soft tissue complex. The parameters for these materials were then evaluated

using inverse FEA based optimization to match the force boundary conditions from experimental indentation tests. A custom designed robotic *in-vivo* indentation system capable of loading the residuum at controlled rates is used to acquire a rich experimental data set of corresponding force versus time at 18 different anatomical locations across the residual limb. The tissue non-linear elastic material behavior was modeled by hyperelastic and 2nd order Ogden formulations while viscoelasticity was added through the quasi-linear theory of viscoelasticity. The experimental force versus time curves obtained for controlled load rates from the robotic indentation system are used as boundary conditions (load curves) for the inverse FEA based material parameter optimization. To determine the material parameters of the residual limb, an optimization routine is used that minimizes the difference (the combined mean of the squared force differentials) between the numerical and experimental force-time curves at 4 distinct anatomical regions on the residuum. The further evaluate the predictability of the FEA model, with optimized parameters for the two tissue layers, the experimental force-time curves for the remaining 14 anatomical locations were then predicted and compared to the experimental measurements. The predictive and patient specific model of the residuum presented, featuring material parameters evaluated based on in-vivo indentation, may prove critical to the future advancement of quantitative methodologies for prosthetic socket design.

2.2. METHODS

All data processing and visualization was performed using custom MATLAB (R2015a The Mathworks Inc., Natick, MA) codes and the open source MATLAB toolbox GIBBON (r89, (31,32), http://www.gibboncode.org/). FEA was implemented using the open source FEA software FEBio (33) (version 2.1.1, Musculoskeletal Research Laboratories, The University of Utah, USA, http://febio.org/).

2.2.1. Experimental methods

To accurately characterize the biomechanical behavior of the residuum through inverse FEA, three distinct processes were integrated. Firstly, surface and internal geometry data of the residuum were captured via non-invasive MRI of the residuum while MRI compatible skin markers were attached at 18 selected locations. These locations of the markers were informed by two main reasons: 1) specific locations of relevance in prosthetic socket design (for example, patellar tendon, fibula head, distal tibia, and posterior wall), and 2) anatomical variance: markers were placed on regions of large muscle thickness, bony regions, as well as medial and lateral points of interest all around the residuum. Surface segmentation of the MRI data provided the geometric input for FEA. Secondly, a custom indentation device was used to record force, time and displacement data for all locations corresponding to those highlighted by the MRI markers. Finally, non-linear elastic and viscoelastic material constants that defined the residuum were identified through inverse FEA based optimization using the boundary conditions derived from the experimental indentation. This section first discusses the MRI acquisitions followed by a description on the indentation experiments.

2.2.2. Magnetic resonance imaging (MRI)

For this study a patient with a bilateral transtibial amputation was recruited (male, age 50, amputation at age 17, weight 77 kg, activity level beyond K3). The amputation of the patient was for traumatic reasons. Informed consent was obtained using a protocol approved by the Committee on the Use of Humans as Experimental Subjects at the Massachusetts Institute of Technology. The patient was placed prone and feet-first inside a 3 Tesla MRI scanner (Siemens Magnetom Tim Trio 3T, Siemens Medical Systems, Erlangen, Germany). All imaging was performed with a RF body coil wrapped around the residuum without causing tissue deformations. An Ultra-short T_E MRI (UTE-MRI) sequence (e.g. (34)) was used, (T_R/T_E=5.8/0.1, acquisition matrix 256x256, 256 slices, voxel size 1.18x1.15x1.00 mm) for image data acquisition.

The indentation experiment was conducted outside the MRI environment. Therefore to highlight the desired indentation sites during imaging, 18 MRI compatible Beekley PinPoint® markers (Beekley Corporation, One Prestige Lane Bristol, CT 06010) were attached to the skin surface prior to imaging. These marker attachment sites were also denoted on the skin surface using body-safe eyeliner. Figure 1 illustrates marker locations on the actual skin surface of the volunteer, and on the skin surface reconstructed from the segmented MRI data. The surface models used in the optimization did not include marker shapes as these were only used to quantitatively identify marker locations.

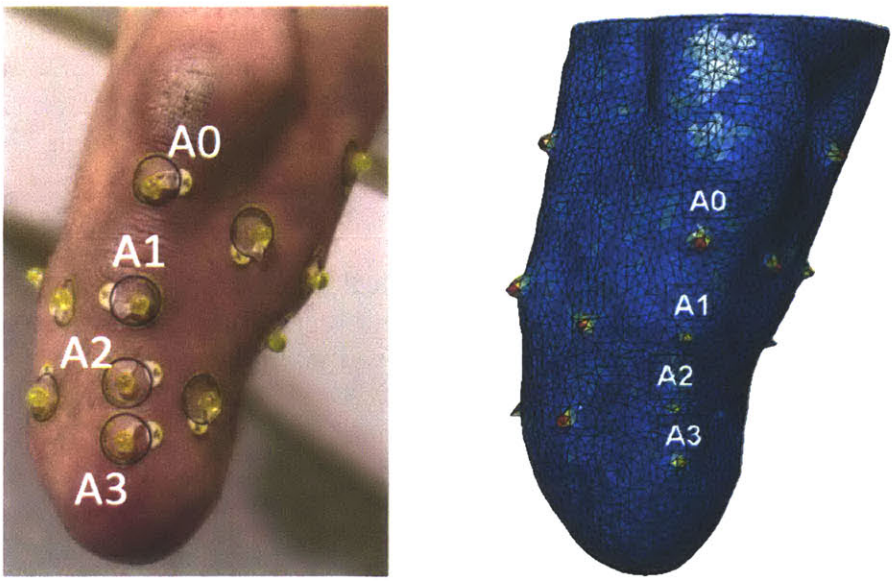

Figure 1: MRI markers placed on the actual skin surface (left) and the corresponding marker regions highlighted on a surface model derived from the MRI data (right). A distance metric is used to quantitatively identify marker locations in the model (red locations corresponds to largest differences between the surface with a marker and the surface without, that is, marker locations)

2.2.3. The indentation experiment

Immediately following MRI, indentation of the residuum was performed for all 18 sites using a custom designed and computer controlled indentation system named FitSocket (see also US Patent (35)). The FitSocket system is shown in Figure 2 and consists of a circular arrangement of 14 indentors. Each indentor head is a 20 x 20 mm non-rounded square block. The surfaces of the indentor heads are equipped with capacitive sensors allowing for detection of skin contact, i.e. moment of touch during loading.

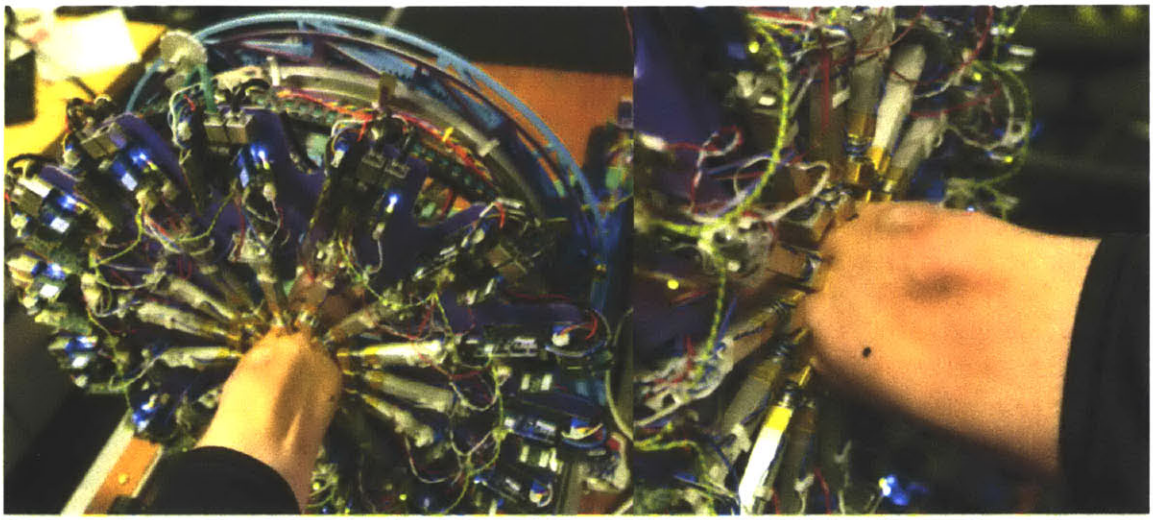

Figure 2: An experimental setup showing a residuum within the FitSocket. Adjacent pins to the test pin (loading pin) are removed from the skin surface to allow tissue displacement

The patient was seated comfortably next to the FitSocket system and asked to insert his residual limb into the device. The FitSocket system was then manually rotated and translated to position one of the indenters orthogonal to the skin at a test site. While the indentor positioned at the test site, called the test indentor, and its adjacent two indenters were held static (and were not touching the residuum) the other 11 indentors clamped the limb with an operator-selected force generally between 14 N and 16 N. The two adjacent indenters stayed removed from the skin surface to allow the tissue surrounding the indentation site to bulge during the indentation. Following clamping, all indentors were held in place while the test indentor was then activated to move towards its starting position to just touch the skin. This start position was determined by monitoring the indentor capacitance and force sensor data. Next, the maximum indentation depth was determined by slowly activating the indentor (at a rate of 5 mm/s) up to a maximum comfortable indentation level. This step allowed for the maximum achievable indentation depth to be set while patient discomfort was avoided. After recording this initial indentation used to set the maximum depth, the indentor was retracted to its initial starting position. A pause time of 5 s was then maintained to remove some pre-conditioning effects due to the initial test indentation. Then a single indentation was performed for the test site at a constant indentation speed 0.96 $\pm$0.5 mm/s. Although a constant indentation speed was used for all sites, local thickness variations meant that varying indentation depths and therefore strain

rates were tested across the residuum. The experimental loading direction was such that during indentations, the flat surface of the indentor was always normal to the skin. As such, loading direction changed slightly during experimental indentation. During indentation, time, displacement and force were recorded at 500 Hz. Figure 3 shows a typical raw and regularized experimental force-time, force-displacement and displacement-time data. Regularization was performed to suppress the minor effects of noise. The regularized curves for displacement and force were derived from linear fitting, and cubic-smoothening spline fitting respectively. During regularization, the loading and unloading parts of the curve were treated separately (hence peak force is not smoothened).

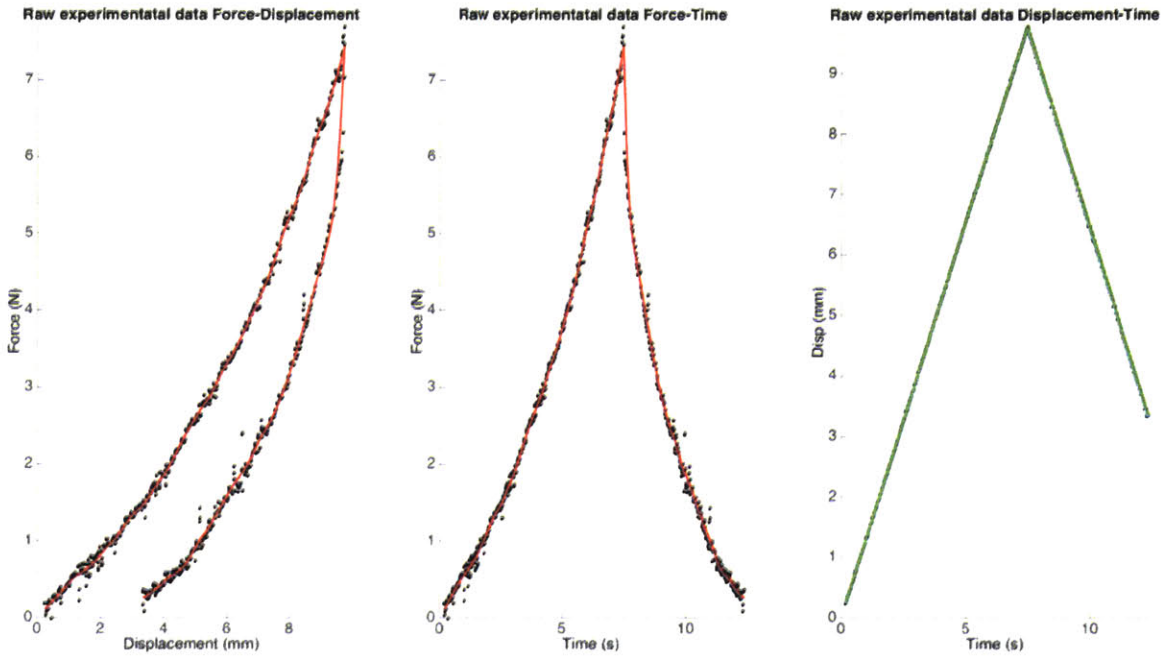

Figure 3: Typical raw FitSocket indentation experimental data. From left to right displacement-force, time-force and time-displacement curves are shown. Black dots denote the raw data while the solid curves are regularized curves.

The above initialization (orientation, alignment and maximum depth setting), indentation and regularization process was repeated for all 18 marked indentation sites.

2.3. Computational modeling

2.3.1. Finite element model construction: MRI segmentation → surface generation → meshing

For this study, tissue contours for the skin surface, muscle, and bones were segmented from the MRI data (based on GIBBON (31) *uiContourSegment* function). These contours were then converted to triangulated surface models. The two solid material regions modeled were: 1) skin (epidermis, dermis, and

hypodermis/adipose layer), and 2) the remaining internal soft tissue (predominantly skeletal muscle and adipose tissue). The bones were represented as rigidly supported voids. The average thickness of the skin-adipose layer was observed to be 3 mm (consistent with thicknesses reported and used elsewhere (23,36–38)). Therefore, for simplicity the skin region was created with a homogeneous thickness of 3 mm by offsetting the outer skin surface inwards based on surface normal vectors. The solid material regions where meshed with 4-node tri-linear tetrahedral elements using TetGen (version 1.5.0, www.tetgen.org, see (39)) integrated within the GIBBON toolbox. The mesh density varied as a function of proximity to the indentation site with the smallest volume for elements close to the indentor and largest volume for those furthest away from the indentor. Mesh density was increased until the predicted indentation forces were no longer dependent on the mesh size.

For each of the 18 indentation sites, a dedicated FEA model mesh was constructed. At each site the central point of the flat head of the indentor was placed at the marker location derived from the MRI data. The indenter geometry, derived from its CAD design, was meshed using 5922 triangular shell elements and modeled as a rigid body. The indentor loading orientation orthogonal to the surface of the residuum was determined from the mean of the local skin surface normal directions. The indentor was then offset from the skin surface to avoid initial contact in the simulation. Figure 4 shows a typical segmented surface geometry and meshed 3-D FEA model geometry with the indentor model.

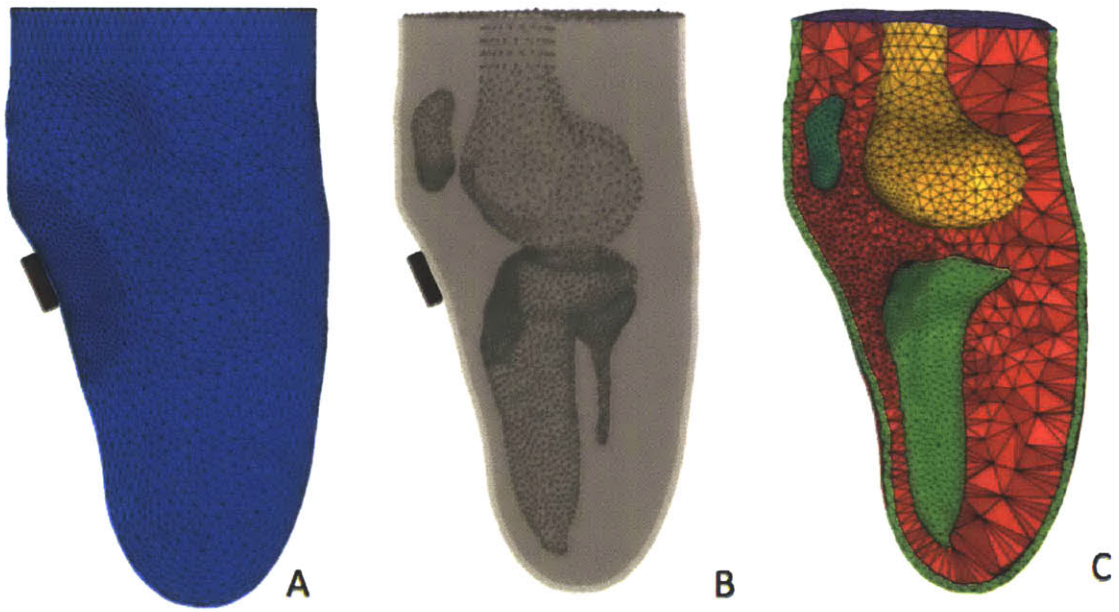

Figure 4: (A) Typical surface model geometry showing local refinement near the indentor (example is for the patella tendon region), (B) transparent surface data showing supported internal surface nodes, (C) a typical solid tetrahedral mesh showing internal refinement as a function of proximity to the indentor. In addition, the two material regions, i.e. the skin-fat layer (green) and the internal soft tissue (red), and the bone voids are visible.

2.3.2. Boundary conditions

The indentation boundary conditions (load curves for loading and unloading) of the simulation for each site were derived from the experimental displacement-time data. Therefore, indentation depth and rate of loading for each site corresponded to the experimental data. The slight variation in experimental loading direction was deemed little and thus it was assumed that the loading direction did not change in the simulation. A zero-friction sliding interface (see FEBio User Manual and also (40–43)) was assumed between the rigid indentor (master) and skin (slave) surface. All nodes of the top surface of the residuum and of the bones were constrained from moving in all directions (see Figure 4B). Hence the bones were represented by rigidly supported voids. Since the indentation sites were far from the top of the model, deformation in those regions were assumed to be negligible.

2.3.3. Constitutive modeling

The indentor was represented as a rigid body material. The soft tissue components were modeled as non-linear elastic and viscoelastic materials. Two soft tissue regions were distinguished: 1) a skin-adipose layer, and 2) an internal muscle-soft tissue complex. The patellar tendon was not separately modeled and was included in the internal soft tissue complex. The continuum mechanical formulations for these materials are briefly discussed below. For a detailed discussion of non-linear solid mechanics and tensor algebra the reader is referred to specialized literature (44–46).

The right Cauchy-Green tensor is given by:

$$\mathbf{C} = \mathbf{F}^{\mathrm{T}}\mathbf{F} \qquad 1$$

Where $\mathbf{F}$ is the deformation gradient tensor. The eigenvalues of $\mathbf{C}$ are the squared principal stretches ${\lambda_i}^2$. For FEA of nearly incompressible materials it is convenient to decompose deformation into deviatoric (isochoric and shape changing) and volumetric deformation. The following deviatoric deformation metrics can be defined:

$$\tilde{\mathbf{C}} = J^{-\frac{2}{3}}\mathbf{C} \qquad 2$$
$$\tilde{\lambda}_i = J^{-\frac{1}{3}}\lambda_i$$

With $J = \det(\mathbf{F})$ the volume ratio.

Elastic behavior

The elastic behavior is modeled using the following uncoupled, hyperelastic strain energy density function:

$$\Psi = \frac{c}{m^2}\sum_{i=1}^{3}\left(\tilde{\lambda}_i^{\,m} + \tilde{\lambda}_i^{\,-m} - 2\right) + \frac{\kappa}{2}\ln(J)^2 \qquad 3$$

Here c, and m are deviatoric material parameters, the former linearly scales the deviatoric response, while the latter controls the degree of non-linearity. This hyperelastic formulation is obtained from a second-order Ogden formulation with the parameters $c_1 = c_2 = c$ and $m_1 = -m_2 = m$ and has the tension-compression

symmetry property $\Psi(\lambda_1,\lambda_2,\lambda_3)=\Psi\left(\frac{1}{\lambda_1},\frac{1}{\lambda_2},\frac{1}{\lambda_3}\right)$ (note this form reduces to a Mooney-Rivlin formulation if $J=1$ and $m=2$).

The volumetric behavior is dictated by the material bulk-modulus κ. The second Piola-Kirchoff stress tensor $\mathbf{S}$ can be derived from (see also (45,46)):

$$\mathbf{S}=2\frac{\partial\Psi}{\partial\mathbf{C}}=2\frac{\partial\bar{\Psi}}{\partial\mathbf{C}}+pJ\mathbf{C}^{-1}=J^{-\frac{2}{3}}\mathrm{Dev}(\bar{\mathbf{S}})+pJ\mathbf{C}^{-1} \quad (4)$$

With $p=\frac{\partial U}{\partial J}$, the hydrostatic pressure, and $\bar{\mathbf{S}}=2\frac{\partial\bar{\psi}}{\partial\bar{\mathbf{C}}}$ is a deviatoric elastic stress. Use was made here of the deviatoric operator in the Lagrangian description:

$$\mathrm{Dev}(\bar{\mathbf{S}})=\bar{\mathbf{S}}-\frac{1}{3}(\bar{\mathbf{S}}:\mathbf{C})\mathbf{C}^{-1} \quad (5)$$

Given the high water content of biological soft tissue, near incompressible behavior is a common assumption. To achieve this, the bulk modulus is commonly set several orders of magnitude higher than the deviatoric stiffness parameters. During all simulations the bulk moduli were therefore constrained to be a factor 100 times higher than the elastic parameter c. This was found to be sufficient to enforce the volume ratio to remain within 1% of unity.

Viscoelastic behavior

Viscoelastic behavior is modeled using the quasi-linear theory of viscoelasticity (see also (47)). For the uncoupled formulations presented, the viscoelastic expression for the second Piola-Kirchoff stress can be written as (48):

$$\mathbf{S}^{v}(t)=pJ\mathbf{C}^{-1}+J^{-\frac{2}{3}}\int_{-\infty}^{t}G(t-s)\frac{d\left(\mathrm{Dev}(\bar{\mathbf{S}})\right)}{ds}ds \quad (6)$$

Here G defines the following (single term) discrete relaxation function:

$$G(t)=1+\gamma e^{-t/\tau} \quad (7)$$

The parameters γ and τ are proportional (units of stress) and temporal (units of time) viscoelastic coefficients respectively. It is clear that according to this formulation under static conditions eventually all viscoelastic enhancement can decay as a function of the viscoelastic parameters allowing equation 6 to reduce to the pure elastic stress defined by equation 4.

2.4. Inverse FE analysis based constitutive parameter optimization

This section describes the inverse FEA based constitutive parameter optimization. The iterative parameter optimization was done using custom MATLAB software capable of: 1) producing FEBio input files with the appropriate material parameters for the residuum-indenter model, 2) starting FEA analysis, 3) importing and analyzing the FEA results, 4) comparing FEA results to the experimental boundary conditions to formulate the objective function, and 5) performing inverse FEA based optimization of the objective function using a chosen optimization algorithm.

The inverse parameter identification employed Levenberg-Marquardt based optimization (implemented using the MATLAB *lsqnonlin* function, see also (49)).

The four indentation sites chosen for parameter optimization were representative of the different anatomical regions of a residuum used in socket design. The patella tendon region is used as a central point of reference in the design of conventional sockets. The tibia region is considerably different from the posterior wall region in geometry and material composition. The latter has a larger volume of soft tissue whereas the tibia region has little soft tissue between the skin surface and the bone. The final evaluation site was the lateral region between the tibia and the fibula. Anatomically, this region is between two bones and geometrically different from the other sites. The rest of the 14 locations distributed across the residuum were used to evaluate the model using the same material constants from the optimization.

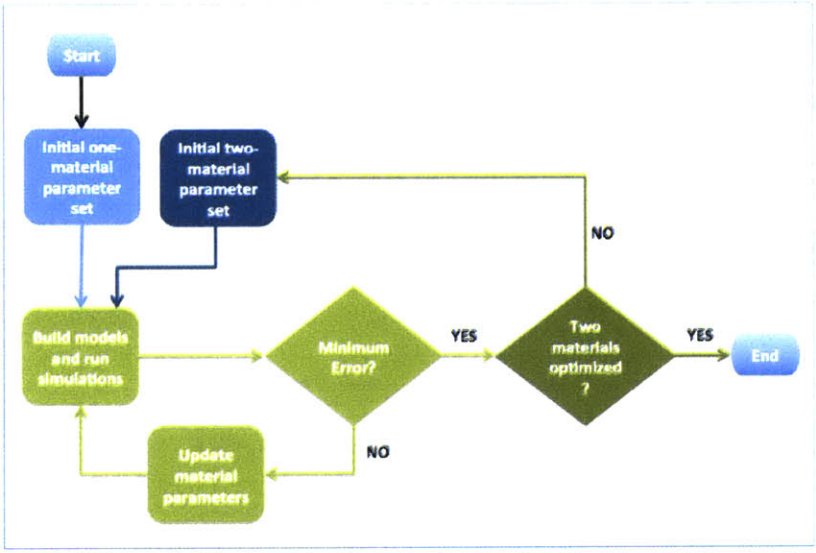

Figure 5: Schematic of two-step optimization routine used for the material constant identification. $c_1 = c_2$, $m_1 = -m_2$ for second-order Ogden

The optimization was done in two stages (see Figure 5). Firstly both tissue regions were treated as one leading to the optimization of four shared material parameters. A second optimization was then performed treating the two tissue regions as separate materials. The initial parameters for this second step were based on the optimal parameters of the first step. The optimization was deemed converged if either the parameters or the objective functions did not vary by more than 0.01.

The objective function vector $\boldsymbol{\mathcal{O}}(\mathbf{p})$ was defined as:

$$\mathcal{O}(\mathbf{p}) = \frac{1}{n}\sum_{a=0}^{n}\left(F_{\exp_a}^{(i)} - F_{\mathrm{sim}_a}^{(i)}\right)^2 \qquad 8$$

Here $F_{\exp_a}^{(i)}$ and $F_{\mathrm{sim}_a}^{(i)}$ are experimental and simulated forces respectively, and i and a denote indentation site and time point indices respectively. Therefore $\boldsymbol{\mathcal{O}}(\mathbf{p})$ is a vector whereby each entry reflects the squared differences of one of the four indentation sites. During the first step of the optimization procedure, a single material behavior is assumed leading to the material parameter vector $\mathbf{p}$:

$$\mathbf{p} = [c \quad m \quad \gamma \quad \tau \,] \tag{9}$$

After convergence of this initial step, the two material optimization employs the parameter vector:

$$\mathbf{p} = [c_s \quad m_s \quad \gamma_s \quad \tau_s \quad c_m \quad m_m \quad \gamma_m \quad \tau_m] \tag{10}$$

The subscripts s and m denote parameters belonging to the skin-adipose layer, and the muscle-soft tissue complex respectively. For the optimization, the parameter bounds were:

$$\text{minimum } \mathbf{p} = [c_s/100 \quad 2 \quad 0.01 \quad 0.01 \quad c_m/100 \quad 2 \quad 0.01 \quad 0.01]$$
$$\text{maximum } \mathbf{p} = [c_s * 10 \quad 20 \quad 10 \quad 10 \quad c_m * 10 \quad 20 \quad 10 \quad 10]$$

2.5. RESULTS

2.5.1. Dedicated and patient-specific FEA modeling of the residual limb

The residuum evaluated in this study was a patient-specific model with all easily distinguishable anatomical features including the surface of the skin and all the bones. Such an FE model could be used in the future to evaluate socket design and internal tissue deformations to understand the effects of surface loading on various anatomical features. In Figure 6, three different meshed models of a residuum are shown with bones (patella, tibia, femur are shown) represented as surface voids, a skin-adipose layer and an internal muscle-soft tissue volume meshed with tetrahedral elements. These models were for indentations at the patella region (left), the tibia region (center) and the posterior wall (right) and they show local mesh refinement for those regions. The residuum model can therefore be customized for different experiments.

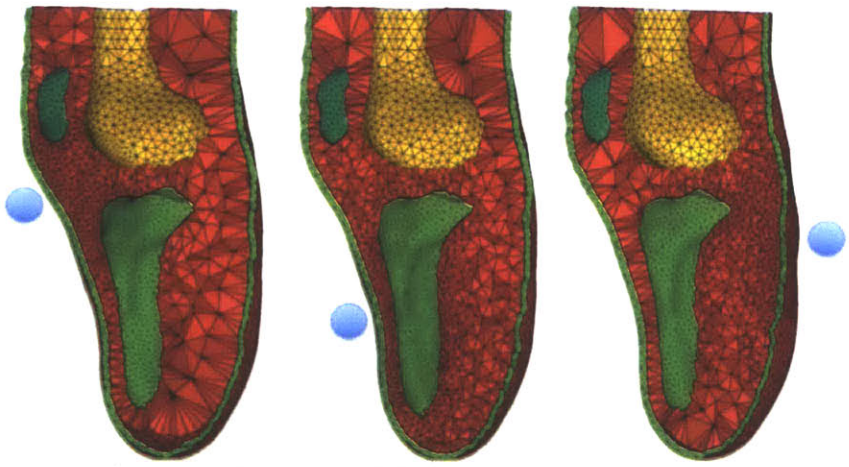

Figure 6: Three complete FEA models showing green elements as skin-adipose layer, bones as voids and red elements as internal soft tissue: patella tendon region (left), anterior tibia region (center), posterior wall (left). Blue markers show finely meshed regions

2.5.2. Inverse FEA based determination of the residuum constitutive parameters

It took between 10-60 minutes for an indentation simulation to converge in FEBio and to import the simulation results for analyses. The results of the optimization with material constants are summarized in Table 1. The optimization was done in two steps (see Figure 5) initially starting with a one material model and then using those optimum parameters as the initial input for the eight-parameter/two material residuum model. Those final optimized material constants presented below were then used to evaluate the mechanical response of the other 14 locations across the residuum.

Tissue type	Material parameter	Initial (4 parameters) One material residuum model	Optimized value (4 parameters) One material residuum model	Optimized value (8 parameters) Two material residuum model
Skin-adipose layer	C_s (kPa)	4.7	5.2	5.22
	m_s	3.00	4.74	4.79
	γ_s (MPa)	1.20	3.86	3.57
	τ_s (s)	2.00	0.31	0.32
Muscle -soft tissue complex	C_m (kPa)	4.7	5.2	5.20
	m_m	3.00	4.74	4.78
	γ_m (MPa)	1.20	3.86	3.47
	τ_m (s)	2.00	0.31	0.34

Table 1: The initial and optimized constitutive parameters for a two-material transtibial residuum model

Table 2 presents a summary of the maximum experimental loading force and the mean percentage error (average mean absolute error/ maximum experimental force) for all 18 indentation sites after the two step material optimization (the four indentation sites used in the optimization are denoted in blue). The force-time and force-displacement curves for the experimental and the simulation data for the four locations used in the optimization are presented in Figure 7 and Figure 8 respectively. For the rigid tibia region, the evaluated displacement is about 3.5 mm. This displacement is doubled at the posterior region, which is mostly soft tissue, and far away from bones.

.

Location	Maximum Experimental Force	1 Material Residuum Model Percentage Error	2 Material Residuum Model Percentage Error	Location	Maximum Experimental Force	1 Material Residuum Model Percentage Error	2 Material Residuum Model Percentage Error
1	8.3	6	6	10	12.31	6	6
2	8.1	4	4	11	11.46	11	11
3	8.8	6	6	12	10.33	4	4
4	15.5	7	6	13	7.46	1	1
5	14.4	2	2	14	7.91	9	9
6	13	5	5	15	10.78	6	5
7	16.7	13	13	16	10.89	4	4
8	12.7	5	5	17	12.21	4	4
9	12.3	11	11	18	11.51	10	10

Table 2: Summary of results after optimization: locations in blue (1,2,12, and 17) were used in the optimization.

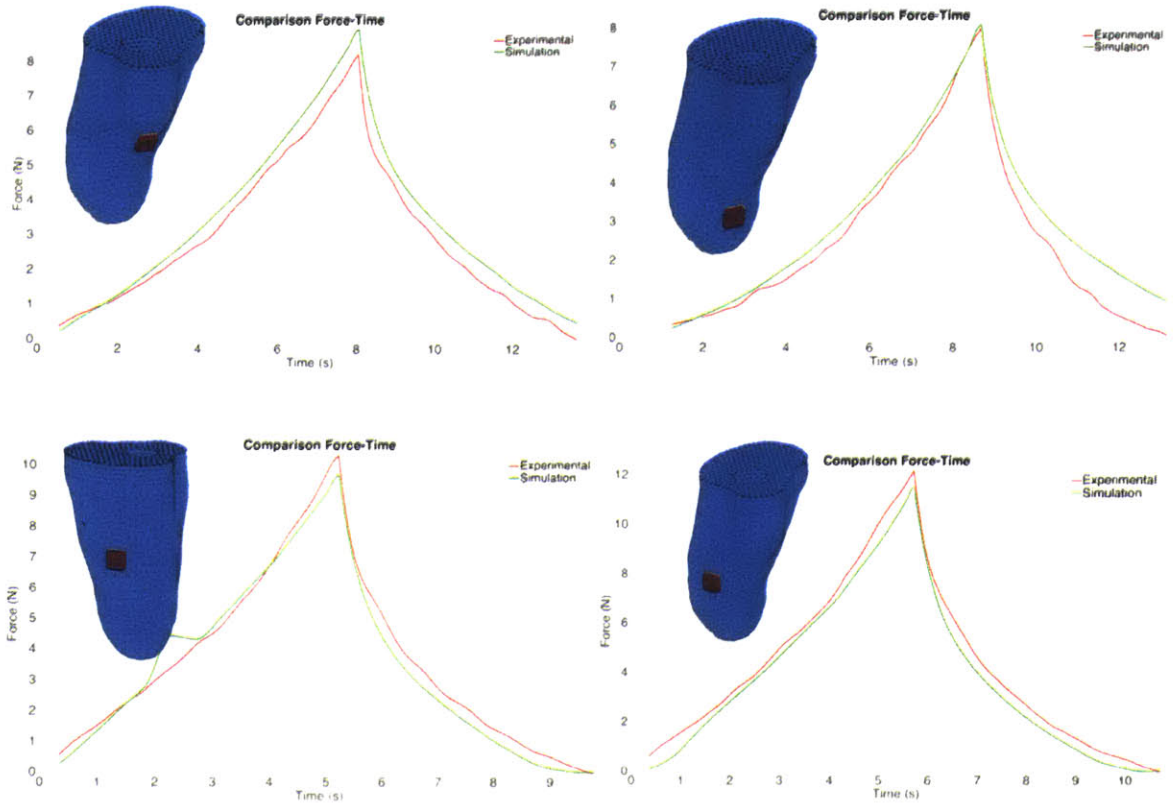

Figure 7: Experimental and a simulated force-time curves at indentation site numbers 1, 2, (top row), 12 and 17 (bottom row) used in the optimization. These are the force-time curves using the material constants from the optimization.

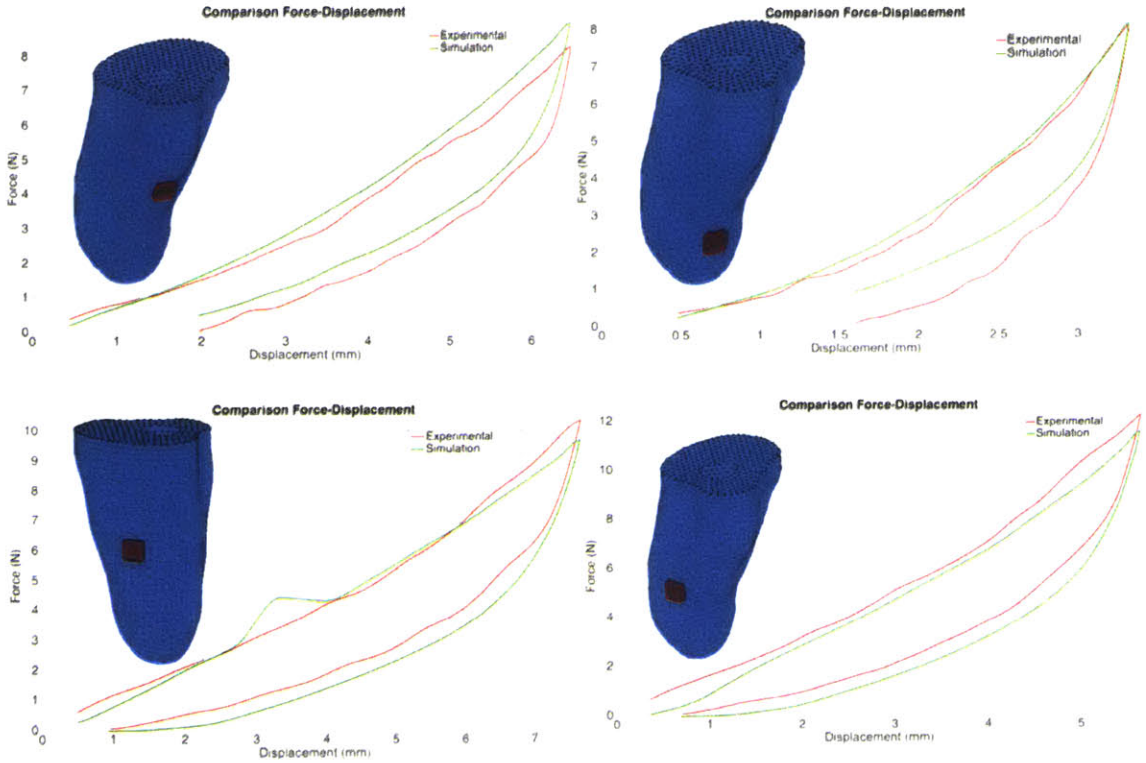

Figure 8: An example of a force-displacement curves at indentation site numbers 1, 2, (top row), 12 and 17 (bottom row) used in the optimization. These results capture the range of predictability for smaller and large displacements

2.6. DISCUSSION

We hypothesized that a computational model composed of two layers of homogeneous materials (i.e. constant properties across the limb) can describe the non-linear elastic and viscoelastic tissue behavior at all anatomical points across the residuum of a person with a transtibial amputation. This paper consequently presented a combined experimental–numerical approach to define material constants for a two-material residuum model. The Ogden material parameters were derived from a non-linear optimization routine that minimized the combined squared differences of experimental and analytical force-time curves across four indentation sites of anatomical significance on the residuum.

The optimization was done in two steps. Firstly, the skin-adipose layer and the muscle-soft tissue complex were defined by the same parameters, and were thus effectively set as the same material. These initial optimized parameters were then used as the initial input from which parameters for a two material residuum model were derived. This staggered approach allows for the evaluation of both a single material residuum model and the investigation of a two material model. For this particular residuum, the mechanical response from the indentations is similar for a single material and a two material model. From these results, it can be concluded that a single bulk soft tissue volume could be used to effectively model the mechanical behavior of a residuum contrary to results reported by Tönük and

Silver-Thorn (2003) (14). While data was recorded *in-vivo* at multiple indentation sites across the residuum in our study and that of Tönük and Silver-Thorn, there are many differences in the approaches for instance in terms of geometry and material formulations used. Tönük and Silver-Thorn performed (non-linear) elastic simulations with 2-D axisymmetric models. In contrast, in the current study, we employed patient specific 3-D FEA and incorporated both non-linear elasticity and viscoelasticity.

There are other *in-vivo* techniques, like elastography, for identifying soft tissue constants on a residuum or a leg. Bensamoun *et al.* (2006) used magnetic resonance elastography (MRE) for characterizing the elastic properties of various muscles on the thigh (50) while Frauziols *et al.* (2015) implemented ultrasound elastography (51). However, for applications in prosthetic socket design, the pressure ranges and displacements for their models are predictive are not sufficient. Recorded pressure readings seen in prosthetic sockets (29) are about 150 times higher than those for which the Frauziols *et al.* model was predictive (20 mmHg). Unlike in other diagnostic scenarios, the residuum soft tissue undergoes large non-linear displacements during socket loading and as such we could not use the assumptions of small deformations with an approximated linear elastic response presented by Bensamoun *et al.* Our methodology uniquely combines: 1) non-invasive imaging, 2) patient-specific segmentation and FEA modeling, 3) a custom designed robotic and *in-vivo* indentation device, and 4) an inverse FEA based optimization of non-linear elastic and viscoelastic material constants for large displacements and stresses at various anatomical locations.

Comparison of the derived tissue material parameters to other studies is difficult due to the differences in methodology, tissue type, species of investigation, modeling approaches and constitutive formulations implemented. However we will briefly discus other literature on soft tissue mechanical behavior. Van Loocke *et al.* (2008) described analysis of the transversely isotropic, non-linear elastic of excised porcine skeletal muscle tissue for *in vitro* compression using the strain dependant Young's moduli approach extended with Prony series to capture viscoelasticity (21). Bosboom *et al.* (2001) used a first-order Ogden model to present a set of parameters that described the mechanical properties of skeletal muscle of rat under *in-vivo* compression ($c = 15.6 \pm 5.4$ kPa, $m = 21.4 \pm 5.7$, $\gamma = 0.549 \pm 0.056$ MPa , $\tau = 6.01 \pm 0.42$ s) (19). Lim *et al.* (2011) also presented material constants for a first-order Ogden model for pig skin (thickness of 2 mm) under dynamic tensile loading. Reported results for comparable strain rates were: $c = 20$ kPa, $m = 11$, $c = 8$ kPa and $m = 7$ for loading parallel and perpendicular to the spine of the pig sample respectively (52).

To compare the material constants from these studies, a 10 x 10 x 10 mm cube described by the reported parameters was compressed for 0.5s, unloaded for 0.5s with an additional wait time at the end of 1 s and results evaluated. All boundary conditions and loading conditions were kept constant. Since Lim *et al.* did not have viscoelastic components, we added parameters from our research and not those suggested by Bosboom *et al.* based on the conclusion from Mukherjee *et al.* (2007) that their viscoelastic expansion was not ideal since loading and unloading paths were not the same (53). Our material model for the human skin-adipose layer

has a similar stress history curve to those predicted by Lim *et al.* when the constants for perpendicular loading were used as shown in Figure 9.

Figure 9: Comparing stress history of uniaxial compression for literature Ogden constants for skin

There is a noticeable difference in magnitude of stress and response decay observed between the rat tibialis muscle and the human muscle-soft tissue complex (Figure 10). Perhaps this is expected since the data is not for human tissue and the composite/bulk response for soft tissue (adipose, tendons, skeletal muscle) is likely different from a skeletal muscle response. Further studies segmenting specific tissues and adipose would be necessary to get parameters for human skeletal muscle undergoing *in-vivo* loading.

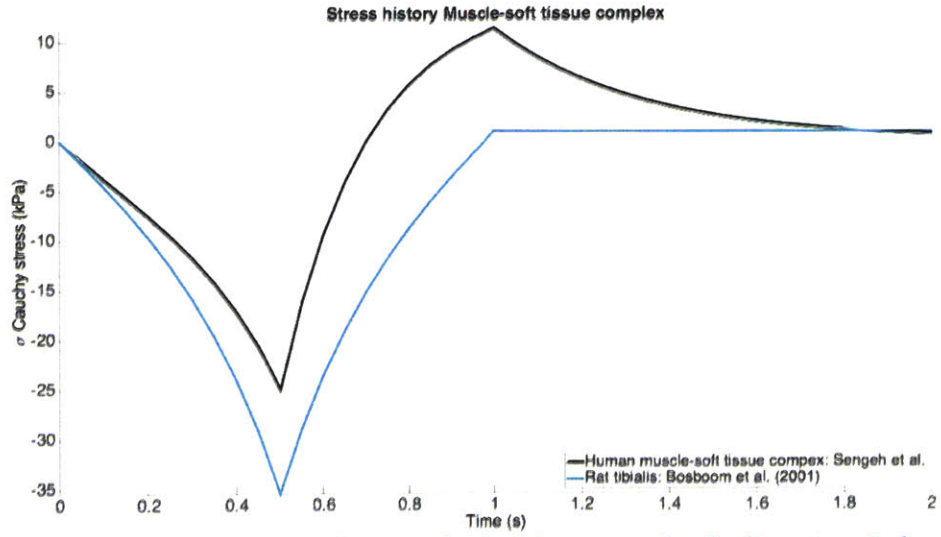

Figure 10: Comparing stress history of uniaxial compression for literature Ogden constants for muscle and muscle-soft tissue complex

The minimum and maximum errors between the force-time curves for the two material model simulation and the experimental setup across the limb were 2% and 13% respectively. The constitutive formulations used to describe the residuum model capture the elasticity, non-linearity and viscoelasticity observed in the residuum at all sites. There is little variation in results between the one material model and the two material residuum models. To better understand this further, more tissue segmentations should be investigated in the future. It must be noted that across the entire residuum, there are at least three regions of distinct biomechanical behavior: patella tendon region, hard body regions (along tibia for example) and soft body regions (in the posterior wall). An additional region would be the anterior medial and the anterior lateral regions, the latter assumed as a load bearing area for conventional socket design.

Tissue type	Material parameter	Initial material constants	Optimized across residuum Model (1, 3, 13, 20)	Optimized across 4 regions on residuum			
				Region 1 1, 10, 11	Region 2 3, 4, 8	Region 3 13, 14, 15	Region 4 5, 6, 20
Skin-adipose layer	c_s (kPa)	4.7	5.22	5.4	5.5	5.1	5.2
	m_s	3.00	4.79	9.86	6.27	4.68	7.55
	γ_s (MPa)	1.20	3.57	2.73	2.64	3.59	1.70
	τ_s s	2.00	0.32	0.45	0.28	0.32	0.38
Muscle -soft tissue complex	c_m (kPa)	4.7	5.20	5.1	4.0	5.2	5.5
	m_m	3.00	4.78	4.52	5.21	4.75	3.85
	γ_m (MPa)	1.20	3.47	2.49	2.66	3.59	3.04
	τ_m s	2.00	0.34	0.35	0.36	0.33	0.40

Table 3: Summary of optimum material parameters for each region compared to parameters across the residuum

The 18 indentation sites were divided into these four regions. Each region constituting one of the locations used to characterize the entire residuum. Eight unique parameters for each region were derived as summarized in Table 3. The average regional errors when all points were separated into one of the four regions were 9%, 7%, 5% and 4% for region 1, 2, 3, and 4 respectively. Whether the parameters were tuned using individual regions or a combination of locations in all regions, the average error was consistent, across the residuum (7%).

In this study, a uniform skin-adipose thickness of 3 mm was assumed. This layer was a combination of the thin and stiffer epidermis and the thicker softer underlying adipose tissue. In the future, it would be worth segmenting the adipose layer from the skin layer particularly where the distribution of fat is not homogenous. The biomechanical behavior of skin and adipose tissue are very

different and this may not be accurately reflected in the current combined form. Conclusions from Portnoy *et al.* (2006) indicate that presence of scar tissue, for example, can inform a more predictive patient-specific model (54). Such peculiar geometries and other anatomical features like connective tissues would be segmented for modeling.

Furthermore, it may be better for socket design if the patella tendon segmentation was included in the residuum model since most prosthetic socket designs rely on loading this tissue. Adding the stiffer patella tendon would potentially enhance the local force response for the computational model. However, at present, the match is already within 6% at this location. Tissue anisotropy should also be considered for future modeling. It also remains to be investigated whether muscle tone is an important feature and if local scarring or internal tissue adjustments may be relevant. As such active muscle modeling and spatially varying mechanical behavior can be included can be included in future work.

In defining the boundary conditions, a limitation and source of error was the direction of motion for the indentor. For the current indentation device the indentor heads are not rigidly attached to their shafts but are instead able to alter their orientation somewhat during loading. This effect was not modeled and may have influenced the results for regions of high curvature where orientation changes may be expected like the fibula head region. In future experiments, the experimental loading direction must be quantitatively tracked using markers on the surface of the indenter and the residuum or a different rigidly attached indentor head needs to be installed. Other boundary conditions that affect convergence and the results of the simulation include contact conditions and the material bulk-modulus (κ). In this optimization κ was set as 100 times the c parameter, which was sufficient to enforce the volume ratio to remain within 1% of unity. With this value, there was convergence at all evaluated locations on the residuum.

The indentor geometry contains sharp edges and corners, which caused convergence difficulties for some simulations. In areas of high curvature on the residuum, it was more difficult to capture data because of the indenter shape and size. In this case, a spherical and smaller indenter would provide better data for loading around uneven surfaces. The indentor geometry also required a relatively high mesh density to allow the tissue to conform to these edges during indentation. For coarse meshes, penetration at these edges was observed, as the tissue mesh was unable to capture the edge geometry. As such to improve model convergence and potentially reduce mesh density (and therefore computational time), a smoother indentor geometry, such as a sphere, would be more desirable.

A zero-friction sliding interface assumption was used in this study. However, when a sticky contact was implemented, the maximum simulation forces did not vary significantly.

A further limitation in the evaluation presented here is the lack of validation of tissue deformation. Future work should incorporate the use of surface deformation measurement techniques, e.g. based on digital image correlation (55). Alternatively, indentation experiments can be combined with simultaneous non-invasive imaging techniques such as MRI (56). Such an approach would allow for the assessment of tissue geometry, and 3-D soft tissue deformation (57,58), and can also

be combined with MRI based assessment of muscle fiber architecture (59). This would allow for the detailed evaluation of the non-linear internal deformations as well as anisotropic material behavior. For future work, since the methodologies presented here are repeatable and use MRI data, we will model and evaluate other patient-specific residual limbs to better understand how these material constants vary across patients.

2.7. CONCLUSION

An important step in the process of quantitative prosthetic socket design is the development of a predictive biomechanical model of the residuum. This paper presents such a model for a single patient featuring non-linear elastic and viscoelastic constitutive behavior of residuum tissues. The model geometry was derived from non-invasive imaging and the constitutive parameters were evaluated based on *in-vivo* indentations. Although the inverse FEA optimization was based on only 4 distinct indentation sites on the residuum, the model was able to provide indentation force predictions for the remaining 14 sites on the residuum to within 7 $\pm$ 3 %.

3. Chapter 3: Study II

Assessment of non-linear viscoelastic constitutive properties of seven transtibial residuum models

*David M. Sengeh, Kevin M. Moerman, Arthur Petron, Hugh Herr**

Center for Extreme Bionics, Massachusetts Institute of Technology, Cambridge, MA, USA

Abstract

The design of quantitative prosthetic sockets requires the accurate biomechanical model of a residual limb. Using computational modeling combined with *in-vivo* indentation experimentation, and digital imaging, a biomechanical model, which captures the non-linear elastic and viscoelastic response of residual limb could be identified. This study evaluates the biomechanical response from indentations at multiple locations on seven distinct transtibial residual limbs described by the same theoretical modeling framework. A non-linear hyperelastic and viscoelastic material law is used to describe the soft tissues within the models. Experimental data of force, displacement and time, were captured on the residual limbs using a custom indentation device at unique anatomical landmarks including the patella tendon, fibula head, tibia, and posterior wall regions. The residuum model geometries were developed from MRI data and composed of all bones, and a skin-adipose layer linked in series to an internal muscle-soft tissue complex. The participants were all active healthy males living with amputations for at least nine years. A single set of material constants for a bulk soft tissue response was derived from an optimization on a single residuum, which minimized the combined mean of the squared force differentials between the numerical and experimental force-time curves at four locations. Using that derived single material law; the average percentage error for the force-time curves (average mean absolute error / maximum experimental force) for indentations at multiple locations across all seven limbs was 7 ± *1%*. Separate optimization experiments were used to derive material constants for the soft tissues on five of the seven residual limb models. Using the patient-specific material constants, the average percentage error was 6 ± *1 %*. There are two conclusions from this study: 1) a single theoretical framework can be used to develop residuum models for patients with transtibial amputations, and 2) while a single set of material constants can generally predict the biomechanical response at multiple locations on a transtibial limb, a patient-specific material constant optimization can improve model performance. The difference between the mean absolute errors of the force-time curves across the limbs using a single material constant and those predicted by patient-specific material constants is significant (*p-value* = 0.15).

Key words:
Transtibial residual limb, soft tissue viscoelastic properties, inverse finite element analysis, patient-specific modeling

3.1. INTRODUCTION

It is largely recognized in the field of prosthetic care that the design of a comfortable socket is important for the prosthetic leg system (60). Conventional socket design for persons living with limb amputations is still artisanal and non repeatable. For the emerging digital and quantitative socket design approaches, a predictive residual limb model is essential (14). However, it is difficult to accurately capture the biomechanical response of tissue *in-vivo* because human soft tissue is non-linear, anisotropic, viscoelastic, and undergoes large deformations (47)(26)(7). A mixed numerical-experimental methodology involving indentation and inverse finite element (FE) analysis has been used to develop and evaluate soft tissue models. Such computational methods particularly in relation to residuum biomechanical models and socket design are well reviewed in literature (61)(62)(63)(16)(64).

In-vivo indentation tests that describe human soft tissue response vary greatly in literature (that is, linear elastic vs. non-linear elastic vs. viscoelastic material laws; 2D axisymmetric vs. 3D surface models etc.). There is in fact no agreement on material constants to describe human skeletal tissue. Studies by Groves *et al.* (2012) and Tran *et al.* (2007) presented *in-vivo* indentation methods for a multilayer skin whose response was described using Ogden material and neo-Hookean material coefficients respectively (23)(24). However, both models were used to describe response of skin on the arm at small forces and deflections. For socket design purposes, models of the residuum must be predictive at large deformations and high loading forces.

Tönük and Silver-Thorn (2003) developed axisymmetric FE models to study the non-linear elastic material properties of seven residual limbs through *in-vivo* indentation. The authors used an optimization, which involved minimizing the normalized sum of square errors to within 5% to attain the material constants for the bulk soft tissue described the Games-Green-Simpson constitutive model. However, conclusions from that study were that the same material constants could not be used to predict tissue response at different sites on the same residuum. Furthermore, the same constants could not be used to predict residuum tissue response at the same sites over time, making it difficult to use such a model for socket design or evaluation of residuum response (14). For computational methods of socket design and modeling, the residuum model must be predictive across its entire surface.

For a detailed review of other soft tissue biomechanical models, Zheng *et al.* (2001) outlined research methods for geometric and biomechanical assessments of residual limbs including data acquisition methodologies (62). The authors also compiled results of material laws for lower limb models in literature and observed incredible differences. Most significantly, they concluded that tissue response varied with "age, testing site, body posture, muscular contraction, biological condition and gender". They further noted that such modeling techniques were yet to benefit clinical prosthetic services.

With recent advances in technology, Moerman *et al.* (2009) investigated *in-vivo* indentation tests, digital image correlation and FE modeling to define bulk material properties of human soft tissue. While the authors proposed new theoretical frameworks that validated a neo-Hookean hyperelastic model, they stated that the method was limited in capturing viscoelasticity of soft tissue (55). MR elastography (MRE) has the potential to combine imaging and tissue modeling and identification. A review by Glaser *et al.* (2012) described the application of MRE to skeletal muscles in general (63). However, MRE has yet to be introduced for modeling of residual limbs to define the mechanical properties of soft tissues *in-vivo.* Consequently, there still does not exist a set of validated residuum models developed through *in-vivo* studies on human patients that capture the large non-linear 3-D elastic and viscoelastic response of soft tissue across its entire surface.

This particular study aims to evaluate the bulk tissue response for seven transtibial residual limbs defined by a single set of optimized material parameters. Those results were compared to the responses observed when patient-specific optimized material constants were used for each residuum. The set of material constants for the constitutive material law was derived through a mixed numerical-experimental and patient-specific optimization using *in-vivo* indentation and magnetic resonance imaging (MRI) based models. We hypothesize that a single model can effectively predict the biomechanical response across the residuum of multiple patients with transtibial amputations. In the optimization method, the combined mean of the squared force differentials between the numerical and experimental force-time curves at multiple distinct anatomical regions was minimized to determine the material parameters of each individual residuum. The material constants and the calculated errors between the force-time curves at the same indentation sites on the six residual limbs for a single material law were compared to errors calculated using each patient-specific material constants derived from separate optimization routines. Each residuum model was developed using the same theoretical framework and consisted of patient-specific geometries derived from MRI including all bones, a skin-adipose tissue layer, and an internal muscle-soft tissue complex. All soft tissue was assumed to be isotropic and homogeneous and the non-linear viscoelastic constitutive behavior was defined by an uncoupled second-order hyperelastic strain energy density formulation as described Moerman *et al.* (65). Conclusions drawn from the specificity of the bulk tissue biomechanical behavior across indentation sites and patients are novel and valuable to soft tissue research. This in turn can inform the quantitative design of prosthetic sockets globally.

3.2. METHODS

For MRI data acquisition, surface segmentation, data processing and visualization, the GIBBON toolbox (r89, (31,32), http://www.gibboncode.org/) for MATLAB (R2015a The Mathworks Inc., Natick, MA) with custom developed codes was used through out the research. FEA was performed using FEBio, a FE software for biomechanics (33) (version 2.1.1, Musculoskeletal Research Laboratories, The University of Utah, USA, http://febio.org/).

3.2.1. Experimental methods

Between three and five locations of distinct regions on seven residual limbs were identified for experimental *in-vivo* indentations. Those locations were all of anatomical interest including the patella tendon, fibula head, tibia region and mid posterior wall. All corresponding points on the residuum were measured and identified on the model for FE simulations. Patient-specific viscoelastic material constants were identified through an optimization routine for a two-material residuum model for each of the residual limbs.

3.2.2. Image data acquisition via magnetic resonance imaging (MRI)

Informed consent and research protocol approved by the Committee on the Use of Humans as Experimental Subjects (COUHES) at the Massachusetts Institute of Technology was acquired for all six patients. One patient was a bilateral amputee, hence seven residual limbs. Each of the patients was of activity level K3 and had been living with amputations for at least nine years. For the imaging procedure, an Ultra-short T_E MRI (UTE-MRI) sequence and an RF body coil was wrapped around the residuum. The participants were prone, and feet-first inside a 3 Tesla MRI scanner (Siemens Magnetom Tim Trio 3T, Siemens Medical Systems, Erlangen, Germany). Figure 1 shows all transparent seven segmented residuum FE geometry in this study with a meshed indentor at the patella tendon region.

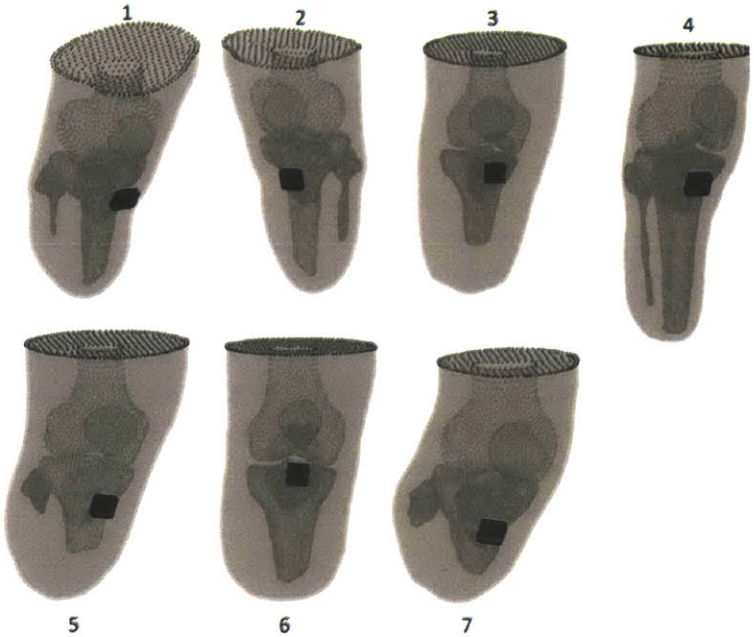

Figure 11: Seven distinct residual limbs segmented from MRI with indentors located around the patella tendon region. Residuum 1 and 2 are from the same patient, Residuum 3 and 6 do not have a fibula bone while residuum 5 and 7 have small fibula bones.

3.2.3. In-vivo indentation

The profile information of the patients included in the study is summarized in Table 4 along with the number of indentation sites on each. The indentation sites chosen were representative of different anatomical regions including the patellar tendon, the tibia and the posterior wall. There was a time range of hours to months between the date of MRI data acquisition and the date of the *in-vivo* indentations among the patients. The custom designed indentor, FitSocket, is shown in Figure 2 with a residuum during indentation. FitSocket consists of a circular arrangement of 14 indentors and each is a 20 x 20 mm non-rounded square block. The alignment of the indentor and experimental data collection methodology were carried out as extensively described in our previous work (Sengeh *et al.* (66)). The loading velocity across all locations on the limbs ranged from a minimum from 0.35 mm/s to a maximum of 2.39 mm/s.

Residuum Number	Amputation Year	Activity level	Gender	# indention sites	Mean indentation Rate (mm/s)
1	1982	K3	Male	3	1.0
2	*1982*	K3	Male	3	1.0
3	2006	K3	Male	4	1.3
4	1993	K3	Male	4	0.6
5	2005	K3	Male	4	0.8
6	1980	K3	Male	4	1.0
7	-	K3	Male	4	1.1

Table 4: Patient/Residuum profiles and # of indentation sites on the residuum

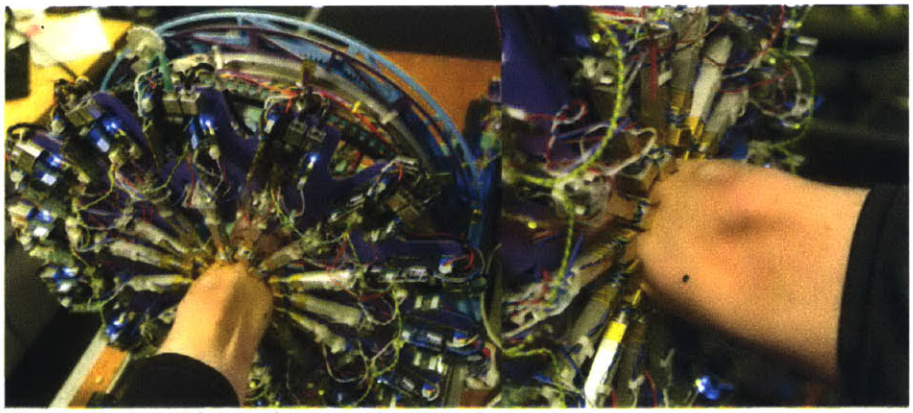

Figure 12: A residuum shown in the FitSocket system

3.3. Computational modeling

Custom developed MATLAB/GIBBON codes were used to segment all soft and hard tissue contours derived from MRI data to create triangulated surface models. Each model was made of bones, a skin-adipose layer, and an internal muscle-soft tissue volume complex. All bones were represented as voids. The thickness of the skin-adipose layer was approximated at 3 mm in all the residual limbs, with the exception of limb #4, which was thinner and estimated at 2 mm (consistent with thicknesses in literature (23,36–38)). The elastic response of the soft tissue components were modeled using the uncoupled formulation of the second-order Ogden derivative constitutive law:

$$\Psi = \frac{c}{m^2}\sum_{i=1}^{3}\left(\tilde{\lambda}_i{}^{m} + \tilde{\lambda}_i{}^{-m} - 2\right) + \frac{\kappa}{2}\ln(J)^2 \qquad 11$$

Where c_i and m_i are deviatoric material parameters, $c_2 = c_1$, and $m_2 = -m_1$. The bulk moduli κ, were constrained to be a factor 100 times higher than the elastic Ogden parameter c, sufficient to enforce the volume ratio to remain within 1% of unity. Viscoelasticity was modeled using the quasi-linear theory of viscoelasticity (see also (47)) and the second Piola-Kirchoff stress can be written as (48):

$$\mathbf{S}^{v}(t) = pJ\mathbf{C}^{-1} + J^{-\frac{2}{3}}\int_{-\infty}^{t} G(t-s)\frac{d\left(\mathrm{Dev}(\tilde{\mathbf{S}})\right)}{ds}ds \qquad 12$$

where G defines the discrete relaxation function:

$$G(t) = 1 + \gamma e^{-t/\tau} \qquad 13$$

The parameters γ (units of stress) and τ (units of time) are proportional and temporal viscoelastic coefficients respectively. All solid material regions where meshed with 4-node tri-linear tetrahedral elements using the meshing software TetGen (version 1.5.0, www.tetgen.org, see (39)) integrated within the GIBBON toolbox. Dedicated FEA models for each site on each residuum were constructed such that the final results in the simulation were independent of mesh density.

All the boundary conditions in the simulations were derived from the experimental displacement-time data with zero friction sliding contact between the rigid indentor (master) and skin surface (see FEBio User Manual and also (40–43)). There was a no-penetration constraint between two surfaces. The nodes at the top surface of the residuum were constrained from moving in all directions. The bones were represented as rigidly supported voids while the indentor was represented as a rigid body material. The indentor was aligned with loading direction normal to the location of indentation.

3.4. Inverse FEA and constitutive parameter optimization

For the inverse FE analysis (FEA) that was used to determine the constitutive parameters optimization for each residuum model, the MATLAB *lsqnonlin* function parameter optimization was implemented. The material constants were considered

optimal when the combined square differences between the numerical and experimental force-time curves at the evaluated indentation sites were minimized.

The objective function for each individual optimization was defined as:

$$\mathcal{O}(\mathbf{p}) = \sum_{N=1}^{N} \left(\lim_{0 \to n} \left(\frac{1}{n} \left(F_{\text{exp,t}} - F_{sim,t} \right) \right) \right)^2 \quad 14$$

$F_{\text{exp,t}}$ and $F_{\text{sim,t}}$ represent the experimental and simulated force for time point index t, n is the number of time points, and N is the number of sites on the residuum used in the optimization. Therefore $\mathcal{O}(\mathbf{p})$ represents the sum squares of the mean force error functions across the indentation sites. The final parameter vector was:

$$\mathbf{p} = [c_s \quad m_s \quad \gamma_s \quad \tau_s \quad c_m \quad m_m \quad \gamma_m \quad \tau_m] \quad 15$$

The subscripts s and m denote parameters belonging to the skin-adipose layer, and the muscle-soft tissue complex respectively. The initial values for the two material optimization for all the limbs were based on an optimization for material constants for a single bulk soft tissue for residuum #1 in Table 4 (where material 1 was similar to material 2). When the convergence criteria were met, the optimal constants for the two-material model were used to calculate the percentage errors between the force-time curves for the simulation and the experimental setup for each residuum. The optimization was deemed converged if either the parameters or the calculated objective function did not vary by more than 0.01.

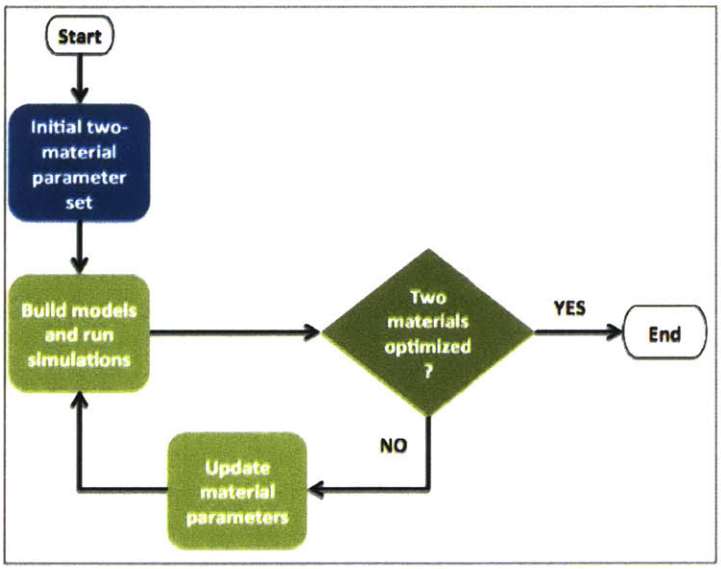

Figure 13: Optimization routine to define material parameters that minimized percentage error for experimental-simulation force-time data.

3.5. RESULTS

3.5.1. Seven patient-specific FEA models of transtibial residual limbs

Seven different patient-specific transtibial residuum models were segmented directly from MRI data. Each of the FE models had unique features (for example, two

residuum were missing fibula bones while another had an elongated fibula), which contributed to a rich dataset for analyses. These models were then used to evaluate material constants across multiple anatomical regions through an experimental-numerical approach. The optimized material parameters are summarized in Table 5.

Tissue type	Material parameter	Initial material constants	Optimized across 6 transtibial residuum					
			Residuum #1	Residuum #2	Residuum #3	Residuum #4	Residuum #5	Residuum #7
Skin-adipose layer	c_s (kPa)	4.7	5.22	5.2	5.2	6.0	5.3	5.3
	m_s	3.00	4.79	4.40	4.66	3.82	4.54	4.65
	γ_s (MPa)	1.20	3.57	3.77	3.84	2.88	3.62	3.60
	τ_s s	2.00	0.32	0.39	0.29	0.96	0.34	0.33
Muscle -soft tissue complex	c_m (kPa)	4.7	5.20	5.2	5.20	6.0	5.3	5.0
	m_m	3.00	4.78	4.38	4.98	2.42	4.64	4.79
	γ_m (MPa)	1.20	3.47	3.68	3.04	4.93	3.59	3.68
	τ_m s	2.00	0.34	0.43	0.33	0.22	0.32	0.33

Table 5: The constitutive parameters for patient-specific optimizations for six residual limbs

In Table 6, we present a summary of the percent error (average mean absolute error/ maximum experimental force) for all indentation sites using a singular set of material constants derived from an optimization routine on residuum #1. In Table 7, for six residual limbs, the percent errors are presented when a patient-specific optimization is run for each residuum. The combined mean percent error reduces to 6% with the biggest reduction on residuum #4.

Residuum #	Indentation site				Mean	SD
	1	2	3	4		
1*	-	-	-	-	7	3
2	2	9	7	-	6	4
3	4	5	4	7	5	1
4	11	9	7	4	8	3
5	10	7	8	-	8	2
6	7	9	7	-	8	1
7	8	10	4	6	7	3

Table 6: Percent error calculated from seven different residuumlimbs using a single material parameter set. The material constants were calculated from an optimization on residuum #1. The error for residuum was calculated from 14 intention locations on the residuum.

Residuum #	Indentation site				Mean	SD
	1	2	3	4		
1*	-	-	-	-	7	3
2	3	8	6	-	6	3
3	4	5	4	7	5	1
4	8	6	7	4	6	2
5	10	7	8	-	8	2
6	-	-	-	-	-	-
7	9	10	3	5	7	3

Table 7: Percent error calculated from patient-specific material optimizations across each residuum. At least three of the four indentation sites were used in the optimization for each residuum.

3.6. DISCUSSION

It is well accepted that human soft tissues undergo large deformations with a non-linear elastic and viscoelastic biomechanical response. In our previous

research, we demonstrated a methodology for evaluating a patient-specific, two-material, 3-D residuum model for a transtibial residuum (Sengeh *et al.* (66)). A combination of non-invasive imaging, *in-vivo* indentation and inverse FEA presented a robust experimental–numerical approach to define material parameters that capture the biomechanical response of residuum soft tissue. The model constituted all bones, and a skin-adipose layer linked in series to an internal muscle-soft tissue complex defined by appropriate constitutive material laws. In this study, we hypothesized that a single set of material parameters optimized on one transtibial residuum would be sufficient to predict the biomechanical response for multiple other limbs. Errors for the experimental-numerical force-time curves at different sites on six patients were calculated. Using similar optimization methodologies, six patient-specific material constants were identified and the calculated errors for the force-time curves at the same locations were compared to those defined by the general material constants (see Table 6 and Table 7).

It was previously concluded by Zheng and Mak (1999) and Tönük and Silver-Thorn (2003) who respectively did linear and non-linear material constant optimization using indentations on the residuum that material constants were dependent on the indentation sites (14)(67). Our results contradict that conclusion. For residuum #1, the mean percentage error calculated between the experimental force-time and the simulation force-time curves was $7 \pm 3\%$ across 14 indentation sites with distinct anatomical compositions (including the patella tendon, anterior tibia, posterior wall, lateral tibia). We used this residuum because we had the most number of experimental data on it. Using the same material constants optimized from residuum #1, there was an average $7 \pm 1\%$ error across 21 locations on six other residual limbs. This indicates that indeed, the second-order hyperelastic constitutive law (65) is capable of closely modeling soft tissues across an entire residuum.

The difference in errors for indentations across the limbs using a general parameter set was significant in comparison to when a patient-specific parameter set was used (*p-value* = 0.15). For residuum #4, the patient-specific parameter optimization reduced the overall errors across the residuum by 2% (see Table 6 and Table 7). As observed from Figure 1, residuum #4 is anatomically very different from the rest of the other limbs. The patient has an elongated and prominent fibula, and is much thinner with reduced fat components in comparison to the other patients. Further studies are needed to better understand the geometries for which a general parameter set will be sufficient to accurately capture the loading response on a residuum. Our results indicate that the absence of a bone does not affect results as much but it appears the size of the skin-adipose layer may be sensitive model characteristic. The optimized constants from these residuum have similar response in magnitude to those material constants for rat muscle and pig skin reported by Bosboom *et al.* (2001) (19) and Lim *et al.* (2011) (52) respectively. However, more investigation in the variations of the material properties and their constitutive relations should be also considered for future studies.

Limitations to our study start with how our models were segmented. An assumption of uniform skin-adipose layer thickness, though informed by MRI data might have a significant role on the constants. As seen with residuum #4, it is

important to accurately segment the skin from the underlying adipose especially where the residuum is thin. In the future, it may be relevant to segment the adipose and the skin layers separately. Experimental boundary conditions varied from the simulation conditions in some instances, which would be a source of error. For example, the loading direction in the experimental setup changed during data collection since the indentor head was not fully fixed. However, the prescribed loading direction in the simulation was kept constant. In the future the loading directions will be tracked using motion capture. Currently, it is difficult to separate the deformation of the skin-adipose layer from the internal soft tissue layer because the indentation is done outside the MRI environment. Internal deformation data would improve the model identification. More complicated components like muscle fiber direction and specific muscle groups can be segmented and modeled.

3.7. CONCLUSION

Identification of material laws that describe the non-linear elastic and viscoelastic response of human soft tissues are essential for FEA and quantitative design of prosthetic interfaces. Here, patient-specific material constants that define the entire residuum mechanical response are derived for seven residuum limbs through an optimization that minimizes errors between the experimental-numerical force-time data. The response across each residuum is then evaluated and compared to response for a general material parameter set derived from a different residuum. The differences are significant and we conclude that patient-specific modeling provides better predictability for residual limbs. Where possible, patient-specific modeling should be used in FEA though the material constants presented in this paper offer a general residuum model characteristic for research.

3.8. ACKNOWLEDGEMENTS

The study was conducted with funding from the Robert Wood Johnson Foundation and the MIT Media Lab Consortium. MRI imaging was at the Martinos Imaging Center at MIT with support from Steven Shannon and Atsushi Takahashi. Other graduate and undergraduate students involved with the research include Bryan Ranger, Daivon Dean and Flora Liu at the Center for Extreme Bionics, MIT Media Lab.

4. Chapter 4: Study III

Novel Computationally Designed Transtibial Prosthetic Sockets

*David M. Sengeh, Kevin M. Moerman, Hugh Herr**

Center for Extreme Bionics, Massachusetts Institute of Technology, Cambridge, MA, USA

Abstract

Conventional prosthetic socket design is artisan, non-repeatable and uses limited quantitative data as input. Consequently, nearly all patients experience discomfort at the residuum-socket interface. In this study, we evaluated three novel computationally designed transtibial sockets at full body weight loading. The surface geometry of the residuum model was derived from non-invasive magnetic resonance imaging data and the material constants were identified via *in-vivo* indentation and inverse finite element analyses (iFEA). To acquire the unloaded shape of the socket, a pressure field derived from a "displaceability map" of the residuum was applied to the liner-residuum model surface. The displaceability map is a spatial representation of how much the residuum deforms at each node under uniform pressure. The mechanical properties of the socket were identified using the said displaceability map, with a goal to reduce the peak contact pressures at critical locations (fibular head and tibia region) on the residuum during full body weight loading. The combination of biomechanical residuum modeling, a quantitatively derived socket shape and spatial socket material property identification through FEA make our design novel. Pressure data at the residuum-liner interface were measured with Teksan F-Socket™ sensors at full body weight standing in the novel and conventional sockets for a bilateral transtibial amputee of weight 78kg. At full body weight loading on residuum #1, % peak pressure change for the novel multi-material socket relative to the conventional socket was -40%, -100%, 0% and -22% at the tibia, fibular head, patellar tendon and posterior wall regions respectively. For residuum #2, % peak pressure change for a rigid novel socket relative to the conventional socket was -23%, -89%, +152% and -57% at the tibia, fibular head, patellar tendon and posterior wall regions respectively. The % peak pressure change for the novel multi-material socket relative to the conventional socket system was -61%, -100%, +338% and -52% kPa at the tibia, fibular head, patellar tendon, and posterior wall regions respectively. The patient qualitatively reported a better fit in the novel sockets compared to the conventional socket. This pilot evaluated a socket designed through an entirely quantitative method with improved comfort for transtibial patients: a foundation for functional CAD/CAM clinical sockets.

Key words:
Transtibial residual limb, CAD/CAM socket design, inverse finite element analysis
*Corresponding author address: MIT Media Lab, 75 Amherst Street, Cambridge, MA 02139, USA Telephone: +16173143661, email: hherr@media.mit.edu

4.1. INTRODUCTION

The number of people living with limb loss is expected to double in the United States by 2050 (1) and the majority of patients are unsatisfied with their prosthetic sockets (2). An uncomfortable socket negatively impacts the ability of the amputee to participate freely in daily activities, including normal gait. At the same time prosthetic socket design is not optimal whether using conventional methodologies or computer-aided design and manufacturing (CAD/CAM) processes (10)(11). The two main conventional socket designs (Total Surface Bearing (TSB) and Patellar Tendon Bearing (PTB) sockets) hinge on the experience of a trained prosthetist and the direct feedback from a patient. The TSB socket interfaces with the residual limb by aiming to apply uniform loads over the entire surface of the residual limb. The PTB socket designs have uneven load distribution by taking advantage of load bearing regions like the patellar tendon and posterior wall of the residual limb as a means to relieve pressure over the distal region and other areas that are not load tolerant, like the fibular head. To design a TSB or PTB socket, a prosthetist wraps a cast around the residual limb of the patient, either in its loaded (under body weight) or unloaded state, using a plaster cast. The positive mold generated from the cast is then modified and used to construct a test socket, from which a final socket is manufactured for the patient (68). This approach of distributing load or contact pressure on the surface of the limb within the socket by adding and removing materials on the positive or negative mold of the residuum is artisan and not repeatable making it difficult for a patient to get comfortable sockets. Both the TSB and PTB sockets are typically rigid and thus apply high pressures on the residuum, leading to discomfort and tissue injury (15).

Computer-aided design and manufacturing (CAD/CAM) tools and technologies have been extensively used in the design of prosthetic sockets to varying levels of success, including those used to capture the shape of the residual limb, to generate positive molds used for socket design and for rapid prototyping of the final sockets (69)(70)(71). To improve comfort, CAD/CAM sockets have typically aimed at lowering high pressures on critical regions (mostly bony protuberances) of the residuum, though these various socket concepts yield non-unique interface pressure profiles (72). The design solutions presented are also varied. For example, Rogers *et al.* (2007) developed double-walled sockets with additional flexible beams over the fibular head and distal tibia region as a means of lowering pressure while achieving structural integrity in transtibial sockets (73). Sengeh and Herr (2013) reported a reduction in pressure at various points of interest on the residuum including the fibular head and tibia region through the design of a multi-material prosthetic socket in comparison to conventional rigid sockets of the same equilibrium shape (74). However, both of these studies relied on an expert human to manually define the socket shape, including the trim line of the socket and neither used an accurate and predictive nonlinear continuum biomechanical model of the residuum in the design process to generate the equilibrium shape of the socket.

The combination of computational modeling with advanced CAD/CAM

techniques is a powerful tool for novel socket design. Lee and Zhang (2007), for example, presented a computational methodology for using pressure and pain evaluated on a residuum model to design better fitting sockets (9). In that study, a limitation was that the soft tissue was modeled using linear material laws. Furthermore, the pressure that leads to pain felt from a single indentor would be different from the pressure field that leads to pain in a socket during full body weight loading. Facoetti *et al.* (2010) also presented computational frameworks for designing sockets, though this requires an active role and significant 'sculpting' by a technician (75). Using Dynamic Roentgen Stereogrammetric Analysis for evaluating dynamic, in-vivo kinematics at the socket-residual limb interface and patient specific finite element modeling, Papaioannou *et al.* (2011) argued that the combination of variable volume socket systems with evaluated vacuum systems had a potential to change the science of real-time, patient-specific prosthetic socket design (76). Portnoy *et al.* (2008) used a series of methodologies (MRI, socket-residual limb interphase pressure sensing, strain and stress measurements) to measure the mechanical behavior and properties of the soft tissue of the residual limb within a socket during static loading conditions (8). The authors suggested that knowledge gained from such analysis could inform the design of prosthetic sockets particularly as it related to understanding potential deep tissue injuries for transtibial amputees. Wu *et al.* (2003) presented a methodology that integrated pain pressure tolerance of soft tissue using FEM for quantitative socket design prior to socket fabrication (77) while Colombo *et al.* (2013) developed a detailed patient-specific socket design and evaluation framework integrated with FEA for reliving discomfort in specific regions on the residuum (78). In instances where FEA was employed in these CAD/CAM designs, the biomechanical models were generally not described by validated nonlinear and viscoelastic patient-specific material formulations of the residuum. Even where the observed advances in tools and processes could be used for prosthetic socket design, there is still no clinical preference for these sockets over conventional ones (79). More alarming is the fact that there is no functional CAD/CAM prosthetic socket whose entire spatial material properties and final shape are truly patient- and load-specific, and dependent on an accurate and validated biomechanical residuum model. Perhaps a reason for this is that in many of the previous studies for which a functional socket was manufactured and evaluated, the authors did not use validated residuum models, inverse FEA (iFEA) and quantitative methods for the liner and socket design and final socket manufacturing to match those designs.

Researchers in the Biomechatronics Group at MIT Media Lab over the last five years have developed a combination of tools for predictive patient-specific biomechanical soft tissue modeling, and automated CAD/CAM approaches for quantitative socket design. Our framework includes accurately modeling the nonlinear response of a transtibial residuum, a custom liner and 3-D printable socket materials. Within that design framework, we apply predictive boundary and loading conditions for FEA, capturing donning and loading conditions of the liner and the socket. We further established a repeatable methodology to identify the equilibrium shape of a socket including the automatic identification of socket cut

lines and the mechanical properties at each surface element of a multi-material prosthetic socket. This current pilot study used the above framework for modeling, design and manufacturing of the evaluated novel prosthetic sockets.

While CAD/CAM has been implemented in prior prosthetic socket research, to the knowledge of the authors, this is the first time a transtibial socket was entirely designed (shape and spatial material property) and manufactured through a continuously quantitative and patient-specific approach. We hypothesize that, using a validated patient-specific biomechanical model of a transtibial residuum, a prosthetic socket could be designed for clinical evaluation such that the socket's equilibrium shape was derived from an applied pressure field on the residuum; and its material property at each surface element area was quantitatively chosen to lower surface pressure on the residuum, particularly at bony regions during standing. We further hypothesize that the pressures at locations near bony protuberances on the residuum during full body weight standing would be lower in the novel rigid and multi-material sockets than a conventional socket system.

4.2. METHODS

Several studies by the current authors and the Biomechatronics Group at MIT Media Lab have described the tools and methodologies used for the socket design evaluated in this manuscript; the custom robotic indentation system used to capture experimental data for residual limb modeling was developed by Petron *et al.* (see US Patent (35)), patient-specific residuum model identification through iFEA as discussed by Sengeh *et al.* (66)), and the automated computational framework used here for socket design was developed by the Biomechantronics Group at MIT Media Lab. All patient-specific MRI data were segmented using the GIBBON toolbox (r89, (31,32), http://www.gibboncode.org/) for MATLAB (R2015a The Mathworks Inc., Natick, MA) and the FEA design performed with FEBio (version 2.3.1, Musculoskeletal Research Laboratories, The University of Utah, USA, http://febio.org/) (33).

4.2.1. Residuum Biomechanical Modeling

From the raw dataset acquired with MRI, surface geometry of all bones and the skin surface were segmented using GIBBON. The residuum was modeled as a bulk soft tissue volume connected to the internal bone geometry. For the soft tissue, the second order hyperelastic material law in Equation 16 was used for its constitutive formulation (see (65)).

$$\Psi = \frac{c}{m^2}\sum_{i=1}^{3}\left(\tilde{\lambda}_i^{\,m} + \tilde{\lambda}_i^{\,-m} - 2\right) + \frac{\kappa}{2}\ln(J-1)^2 \qquad 16$$

$c = c_1 = c_2, m_1 = m, m_2 = -m$, where c and κ have units of stress. The parameter m, which is the degree of non-linearity, has no units and $\tilde{\lambda}_i$ are the principal stretches. The set of material constants for the residuum soft tissue was $[c = 5.22\ \text{kPa} \quad m = 4.4]$ (66). The patellar tendon was also modeled using the same energy density function in Equation 16 with material constants based on human

material testing data by Johnson *et al.* (1994) (80) [$c = 220$ kPa $m = 2$], while the bones were represented by rigidly supported voids.

4.2.2. FEA-based Liner and Socket Design:

This section discusses the analytical design of the patient-specific liner-socket system through FEA. The equilibrium shapes of the liner and the socket were driven by a pressure field applied to the undeformed residuum model with an aim to achieve a reduced interface pressure around prominent bony protrusions like the fibular head and distal tibia regions for body weight loading. The rigid and multi-material novel sockets were modeled with material properties based on the 3-D printable Digital Materials™ from Stratasys (7665 Commerce Way Eden Prairie, MN 55344, USA). For FEA, all bodies were meshed as solid linear tetrahedral elements with TetGen (version 1.5.0, www.tetgen.org, (39)). In this study, a "displaceability map" (i.e. the relative ability of the residuum tissue to locally deform at each node under uniform pressure) was used to identify the equilibrium shape and the spatial mechanical property of the multi-material socket. The liner and socket materials were modeled using the multi-generational material theory (81), which allows the material to have two states during FEA. In the initial state, the materials have negligible stiffness properties and are freely allowed to deform with the residuum under pressure/surface load without building initial stiffness in the material. At the end of this initial stage, before the residuum is allowed to relax back when the load is slowly removed, the liner and socket take their actual mechanical properties (see Figure 14).

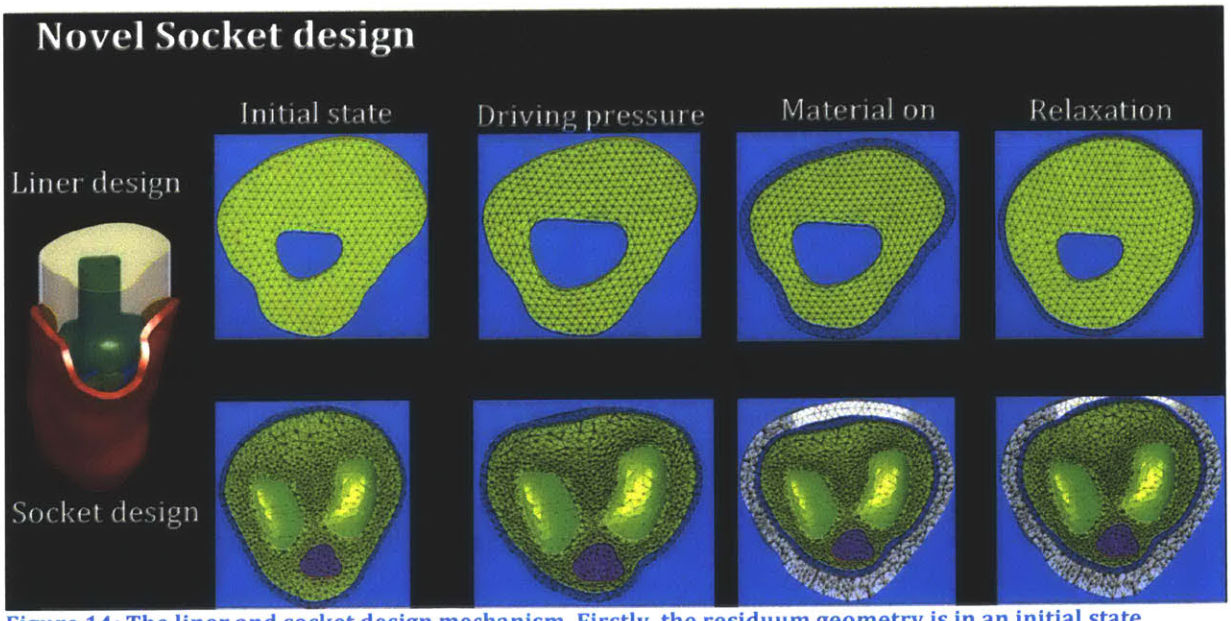

Figure 14: The liner and socket design mechanism. Firstly, the residuum geometry is in an initial state (step 1), which is then deformed by a design driving pressure (step 2). At the end of step 2, the material is given its actual mechanical properties and "donned on". In step 3, the driving pressure is slowly removed as the residuum is allowed to relax within the interface (liner and socket).

4.2.3. Initial shape of liner and socket

To accurately evaluate the socket design framework, a custom liner had to be integrated into the modeling since conventional liners had unknown properties, were not patient specific and they varied in thickness in an unknown manner. The custom liner was designed with a uniform thickness of 3 mm such that the inner layer initially coincided with the undeformed skin surface of the residuum. The socket cut line/trim line was automatically developed using the internal anatomical geometry of the residuum and the initial equilibrium internal shape of the socket coincided with the outer surface of the liner. The socket had a uniform thickness of 8 mm in the model except at the distal region (up to 30 mm above the lowest point on the residuum-liner model) where the thickness was 3 mm. To define thickness, the surface geometry was offset by the desired amount along its surface normal. The entire socket thickness was smoothened after the alterations at the distal end (see Figure 15 for the above described processes).

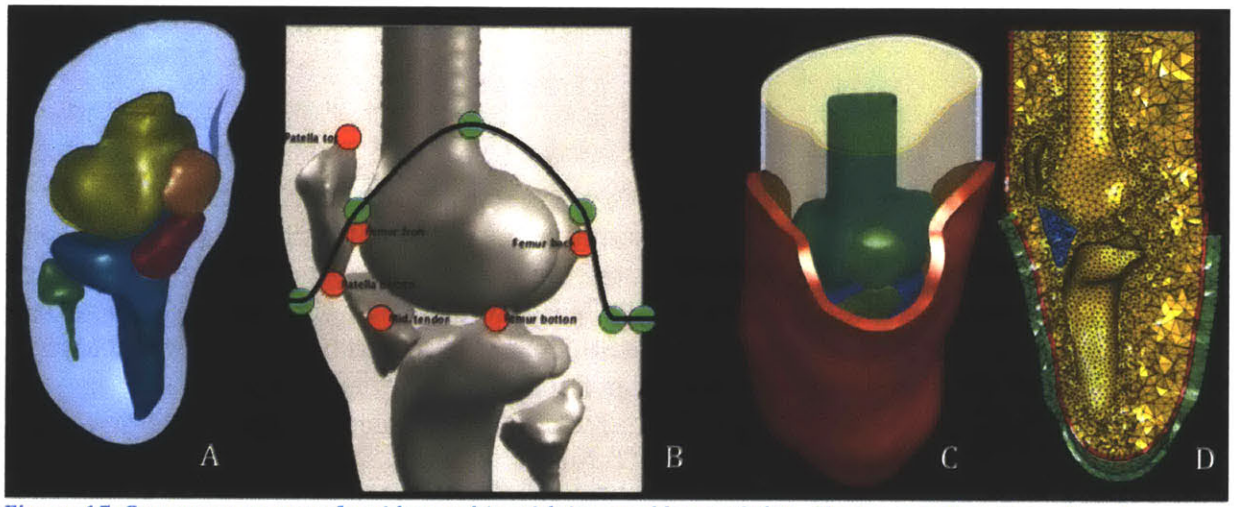

Figure 15: Source geometry of residuum skin with internal bones (tibia, fibular, patellar, femur), and patellar tendon (A). Socket cut line derived from anatomical landmarks (B). A combined socket-liner-residuum model: 8mm thick socket and a 3mm thick liner (C). Combined FE model of residuum, liner and socket with tetrahedral meshes (D).

4.2.4. Mechanical properties of liner and socket materials

For FEA, the liner was modeled as a single homogenous second order hyperelastic material with the following elastic mechanical properties $[c = 0.11\ \text{kPa} \quad m = 4.57 \quad k = 100 * c]$. iFEA and experimental data from material testing were used to identify these optimal material constants for a liner made with Dragon Skin® 10 (5600 Lower Macungie Road, Macungie PA 18062, USA) silicone rubber. Figure 16 shows the stress-stretch curve, which compares the experimental data with a simulated response using the optimized material constants for the liner.

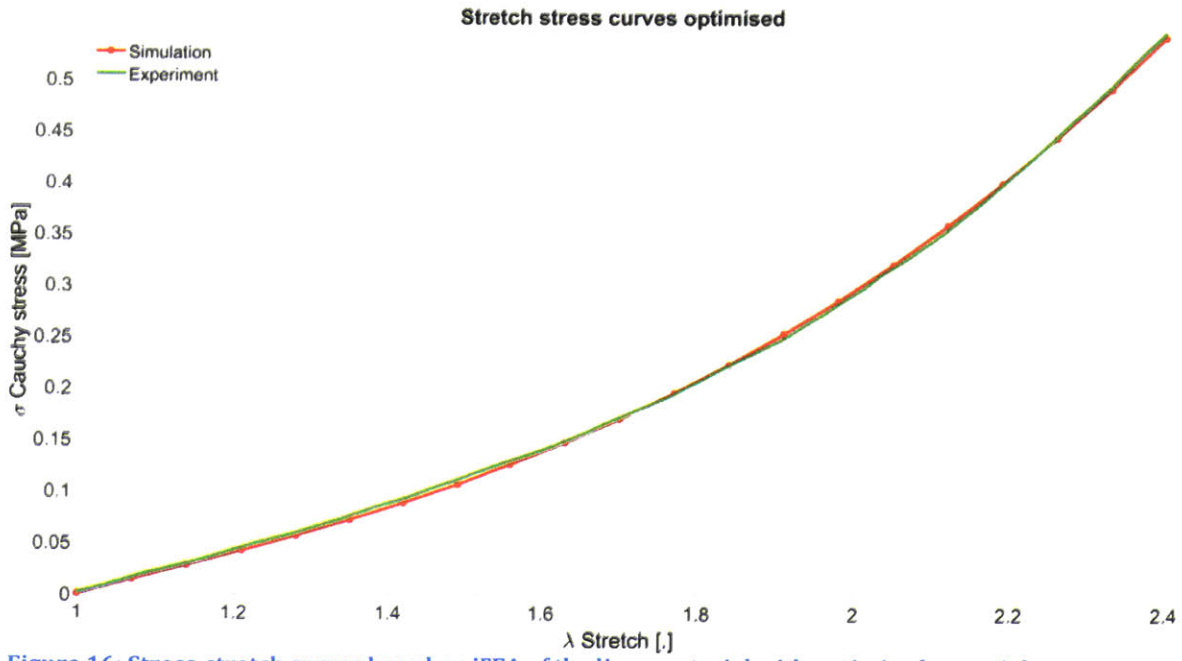

Figure 16: Stress-stretch curves based on iFEA of the liner material with optimized material constants and the experimental material testing data

The displaceability map was used to quantitatively select the mechanical properties of the socket. A linear relationship mapped the stiffest socket materials to the regions of most displaceability while the softest socket materials were mapped to the regions of least displaceability on the residuum. After the global quantitative mapping, the material properties of specific regions (the socket rim, patellar tendon region and distal region) were altered to deviate from the original map. The elements of the socket rim (10mm in height from the cut line) were altered to a material selection that was flexible for donning comfort, while the distal end of the socket was altered to be the softest available material. The socket elements that were within 30mm in distance from the mid patellar tendon were assigned properties of the most rigid material available. Socket elements within 35mm of the fibular head were also altered to be the softest material. The socket material elements were smoothened after these alterations to prevent any sharp material transitions.

The material constants for the Digital Materials™ of the Stratasy Polyjet 3-D printing technology were identified via iFEA using experimental compression and tension loading with (ASTM D638 standards) (see Figure 17 for an example comparative stress-stretch curve between experimental and modeling data). The optimized material constants used for novel socket design are summarized below in Table 8. Since the displaceability map is linear, there is a gap between the suggested socket materials and those available below. As such, for the socket design, all socket elements were grouped with the material that was closest to those suggested by the linear map.

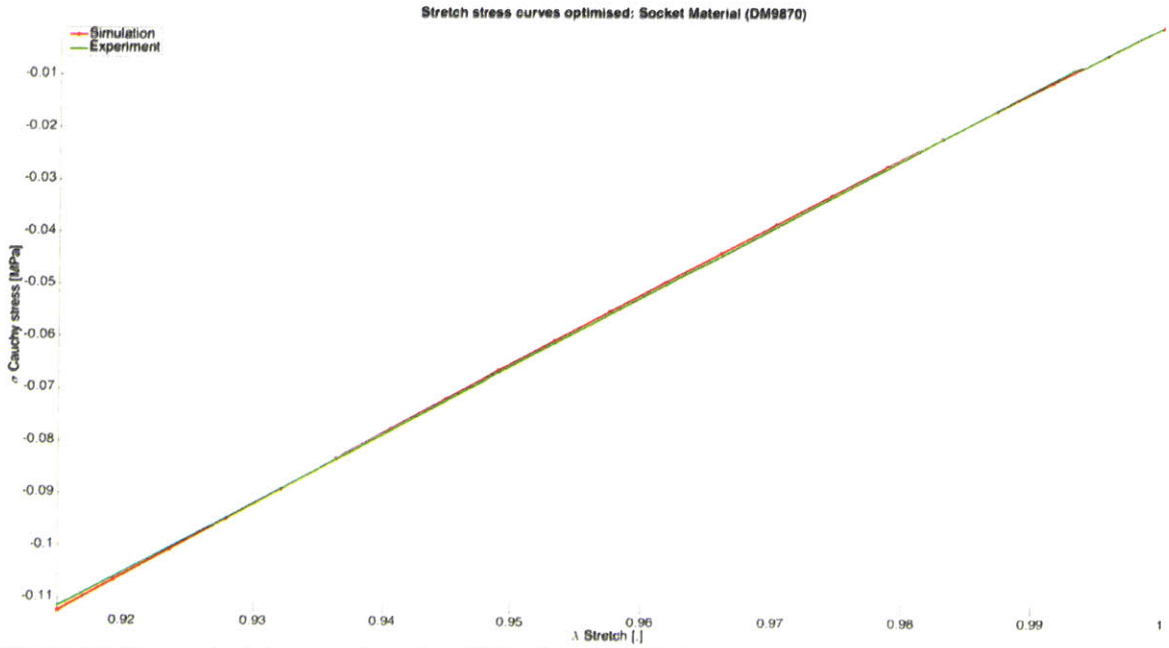

Figure 17: Stress-stretch curves based on iFEA of the DM 9870 material used for the liner with optimized material constants and the experimental material testing data

Digital Material™	Optimized Material Constants	
	c (kPa)	m
TangoBlack+	1.17	2
DM9840	1.62	2
DM 9850	2.04	2
DM 9860	2.80	2
DM 9870	3.41	2
DM 8530	$7.42*10^2$	2
DM 8520	$1.30*10^3$	2
DM 8510	$1.4*10^3$	2
VeroWhite+	$1.39*10^3$	2

Table 8: Material constants for 3-D printing materials

4.2.5. FEA Simulation: boundary conditions, applied loads and steps

For FEA, the nodes that represented bone geometry boundaries were rigidly supported at all stages of the simulation and those at the top surface of the model were constrained from moving in the z-direction. A tied contact formulation was used between the outer surface of the residuum and the inner surface of the liner. To determine the pressure field applied at each node of the residuum, a linear function mapped the minimum and maximum displaceability of the residuum to a minimum liner pressure (15kPa) and maximum (90kPa) pressure. Surfaces that were most displaceable had maximum pressures and those with least displaceability, like bony regions had minimum pressures. In addition, to minimize

distal loading during weight bearing, the pressures at the patellar tendon region were augmented by up to a factor of 6. Meanwhile, in the distal region (all nodes up to 30mm above the bottom of the model) the pressure levels were altered to the minimum, thereby also deviating from the displaceability map. These three regional modifications together combined to achieve minimized compressions and low pressures at critical areas and increased pressure at the patellar region at body weight loading. The FEA simulation was done in three steps:

Step 1: Liner donning

During Step 1, a homogenous pressure was applied to the residuum leading to large deformations of the residuum. The liner and socket were allowed to freely deform with the residuum without building significant material stiffness. To achieve a desirable final average pressure of approximately 15kPa between the skin surface and the liner, a much higher pressure was applied to the residuum. At the end of this liner driving pressure stage, the liner attained its actual mechanical property in the multigenerational state as the residuum pushed back to "relax" while the pressure was slowly removed. The socket was still assumed to have negligible mechanical properties throughout this step. At the final point, the pressure on the residuum was purely from the liner. The shape of the residuum when the liner design pressure was fully applied before allowing it to relax was saved and ultimately used as the positive mold from which the liner was manufactured.

Step 2: Socket donning

During step 2, the liner had its true material properties, while the socket materials were initially still in the state of negligible stiffness. The design-driving pressure field (derived from the displaceability map) used to understand the equilibrium shape of the socket was then applied to the residuum surface, also deforming the limb. At the end of the pressure application phase, the socket attained its mechanical properties and the residuum was allowed to "relax." At this step, the applied driving pressure was slowly removed from the residuum as the limb was allowed to settle in the socket. When a multi-material socket was used, the residuum deforms regions that were soft during relaxation.

Step 3: Loading with body weight

In Step 3, body weight loading was simulated via the application of an upward z-displacement to the supported nodes (the rigid material regions) on the socket surface. The displacement was adjusted until a z-direction reaction force equal to body weight (78 kg for the patient in the pilot study) was obtained. The range of displacement between the supported nodes of the socket and the rigidly held bones to achieve body weight was between 3-15 mm, depending on applied pressure field. For the body weight loading in this experiment, the z-displacement value falls well within displacements measured by Papaioannou *et al.* (2010) while assessing socket-stump kinematics during strenuous activities (18). At the end, contact pressure between the residuum and the liner and the internal strain and stress of the residuum were evaluated.

4.2.6. Liner and Novel Socket Manufacturing

After the above three-step simulation, the coordinates of all elements in the model were saved and imported into MATLAB for analyses. The equilibrium socket shape was the shape of the socket after the application of the pressure field on the residuum in Step 2 before the residuum relaxes. The outer surface of the socket (excluding the nodes at the rim) after body weight loading in Step 3 was thickened to create a rigid outer support structure around the entire socket. Each of the elements was grouped into printable material categories and saved as independent group STL files and sent to the 3-D printer for manufacturing. For the rigid novel socket, the most rigid material was used. It took up to 33 hours to 3-D print each socket. The outer shell, designed for structural integrity was given a base at the distal end for attachment to an ankle system.

The equilibrium shape of the liner was derived such that after donning on the residuum, a uniform mean pressure of approximately 15 kPa was achieved between the liner and the residuum. This surface of the residuum at the end of Step 1 was saved, thickened inwards and 3-D printed to serve as a positive mold from which the liner was manufactured. Dragon Skin® 10 was carefully poured over the positive mold until a uniform thickness of approximately 3mm was achieved. The liner was thus fully patient-specific at equilibrium shape as it fit the contours of the residuum under pressure.

4.3. Evaluation of Socket Pressure:

Interface pressure measurement between the residual limb and the socket was evaluated with the F-Socket™ pressure sensor from Teksan (307 West First Street, Boston, MA 02127). Measurements at specific regions of interest (tibia region, fibular region, patellar tendon, and posterior wall) were recorded during full body weight standing at a frequency of 50 Hz. The sensors were calibrated with a known weight and transfixed to the residuum inside the liner on the residuum with a double-sided tape to prevent sliding (see Figure 18). Pressure readings where taken when the patient stood on one limb in the evaluated socket and then on two limbs. At each instance, the patient stood still for as long as possible without any other support. The readings were recorded for the novel sockets and for the conventional system of the patients. In the conventional system, the patient used his conventional liners and their rigid carbon fiber sockets and for the novel systems, the patient used the custom designed liner with his sockets.

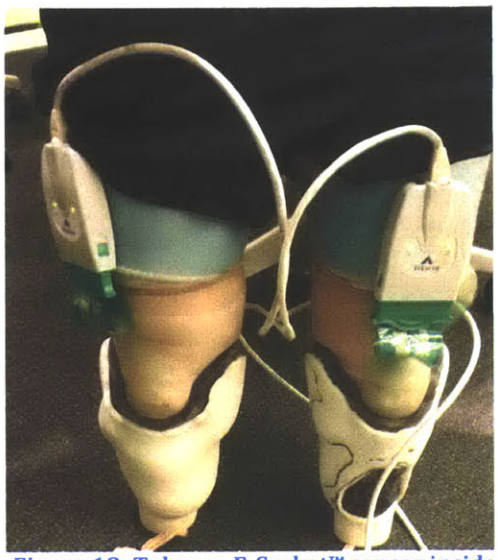

Figure 18: Tekscan F-Socket™ sensor inside a liner donned by a patient.

4.4. RESULTS

4.4.1. Model evaluation and manufacturing

The combined FEA model constituted the residuum (bulk soft tissue, bones, patellar tendon), a uniform liner, and a socket – all forming 409,159 tetrahedral elements. Output data for all elements from the multistep simulation included total deformation, force, stress, strain, and contact pressure at the liner-residuum interface. In Figure 19, contact pressure (MPa) between the surfaces of the residuum and liner is shown as an output on the residuum along with total displacement (mm) as visualized on the entire FEM model. It took between 100 and 300 minutes for the model to converge at the end of the multistep simulation in FEBio depending on the applied loads on the residuum and the boundary conditions used.

The two novel sockets evaluated in this study were designed using quantitative methods and patient-specific anatomical data. One was rigid and the other had spatially varying mechanical properties defined by a linear function linking material stiffness and design pressure to spatial residuum deformability. The multi-material novel socket was shown via FEA to have lower contact pressures on the residuum at bony regions than the rigid novel socket at full body weight loading. The highest pressures in the novel sockets (by design) were concentrated at the patellar tendon region (see Figure 20) as a means of achieving the design objectives.

The results of the simulation for the liner and its consequent manufacturing are presented in Figure 21. In the simulation, the residuum undergoes significant deformations in Step 1 in the design process to represent the equilibrium shape of the liner before it was donned on. The shape of the residuum was saved into an STL

format for 3-D printing of the positive mold. Using a pour over method, a 3mm uniform thickness liner is manufactured over the printed mold.

The equilibrium shape of the socket was derived in Step 2. The liner-residuum model was deformed by the design-driving pressure field while the connected socket material freely deformed in a stress-free state. That socket shape was saved for manufacturing before the residuum was allowed to relax in the socket as the design pressure was removed. An outer rigid support was derived after body weight loading at the end of Step 3, when deformable socket regions underwent further shape change. All the design files were then post processed using 3-matic (v 10.0, Leuven, Belgium) and prepared for 3-D printing. The CAD/CAM process and clinical fitting is shown in Figure 22.

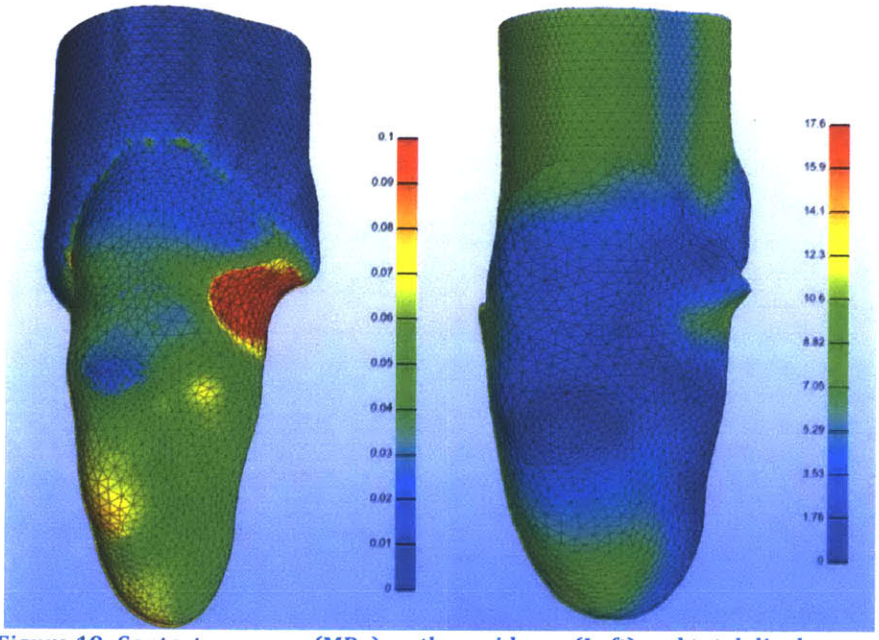

Figure 19: Contact pressure (MPa) on the residuum (Left) and total displacement of the combined model (Right) at the end of the simulation

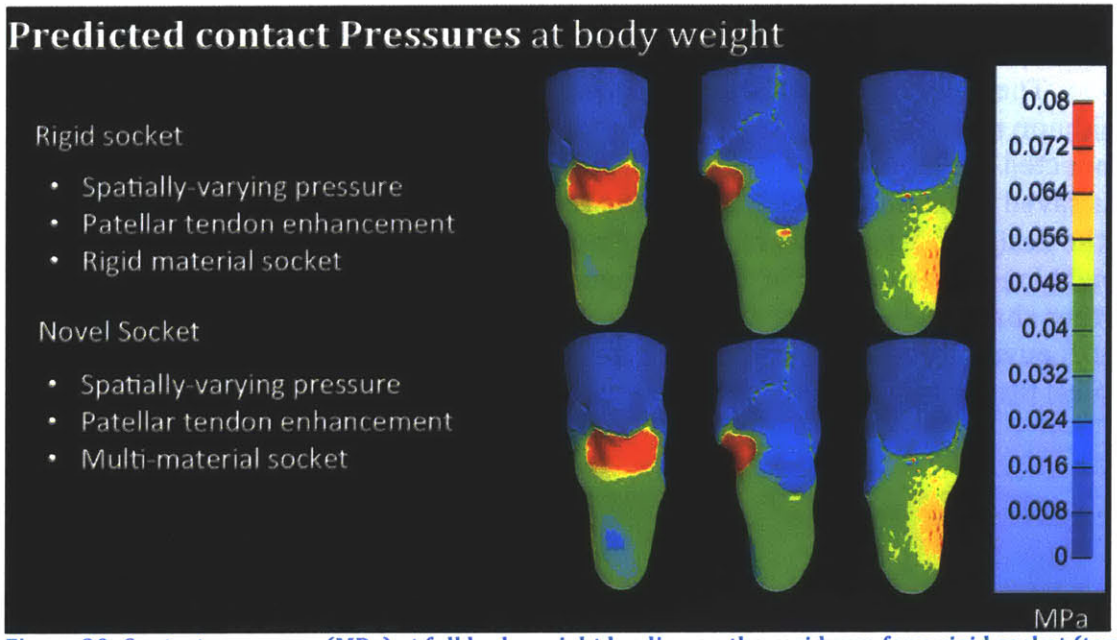

Figure 20: Contact pressures (MPa) at full body weight loading on the residuum for a rigid socket (top row) and for a multi-material socket (bottom row) at the same orientations of the residuum

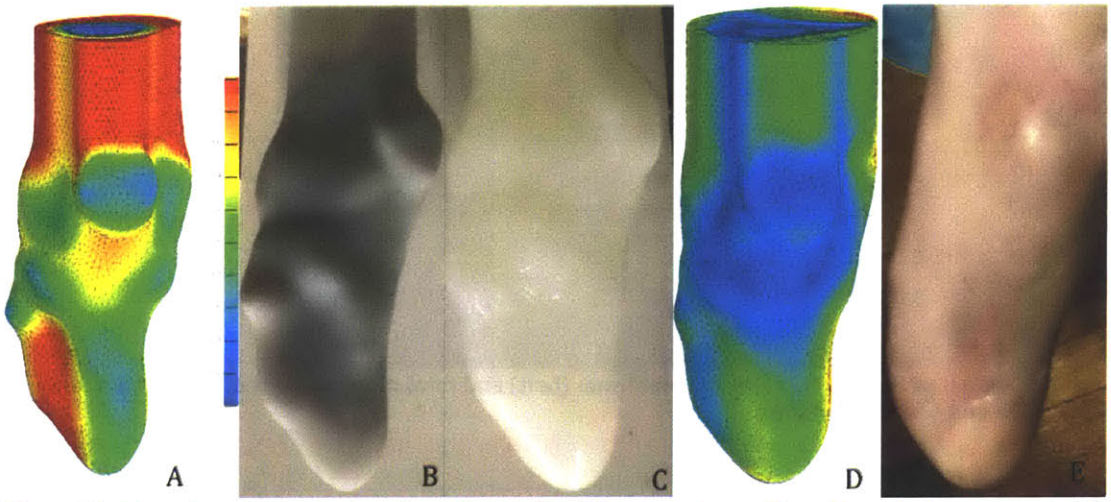

Figure 21: Liner donning and relaxation. Shape of residuum under uniform liner design pressure (A). 3-D printed positive mold of equilibrium shape of liner (B). Manufactured uniform thickness silicone liner (C). Residuum model shape after complete relaxation in the liner (D). Experimental evaluation and donning of the liner with an actual limb (E).

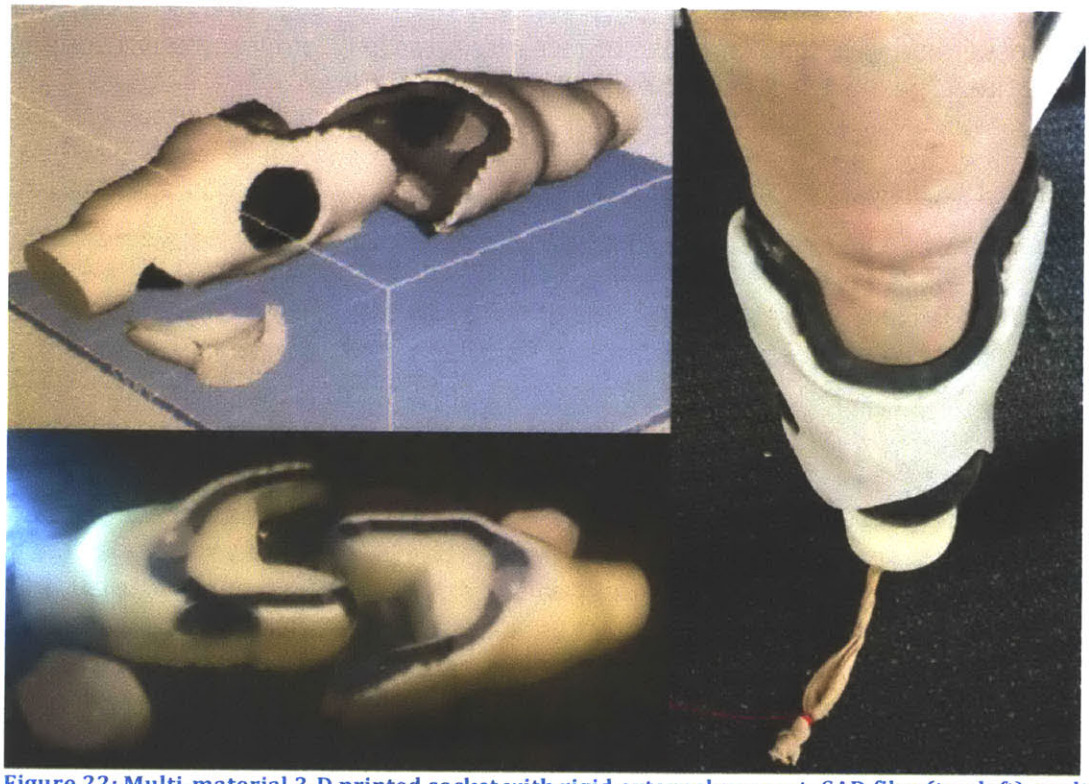

Figure 22: Multi-material 3-D printed socket with rigid external support: CAD files (top left), multi-material printing (bottom left) and a complete liner-socket system donned for evaluation (right).

4.4.2. Interface pressure evaluation

For full body weight loading, the patient was asked to stand on a single residuum with minimal or no support for balancing for as long as he could. For half body weight standing in an evaluated socket, the patient was asked to stand and balance his weight on both legs. This was repeated at least two times and all the stable standing datasets were combined for evaluation. The interface contact pressures at each desirable region for residuum #1 and residuum #2 were averaged and presented below. Figure 23 and Figure 24 are the averaged peak pressure readings at the tibia, fibula head, patellar tendon, and posterior wall regions for full body weight standing for residuum limbs #1 and #2 respectively.

In residuum #1, there are significant reductions in interface peak pressures at the fibular head, the tibia and the posterior wall region of -100%, -40% and -22% respectively between the conventional prosthetic socket and a multi-material novel prosthetic socket (% peak pressure change = ((novel socket pressure –conventional socket pressure)/conventional socket pressure)*100). The patella tendon pressure readings are comparable for the novel multi-material and conventional sockets (see Figure 23). Meanwhile, in residuum #2 (see Figure 24), a rigid novel socket and a multi-material novel socket were both compared to a conventional socket. Pressures over the fibular head and tibia regions are higher in a conventional socket than in the novel rigid socket and the multi-material socket. The novel multi-

material socket had the smallest peak contact pressures over bony regions, though it also had the largest pressures at the patellar tendon region.

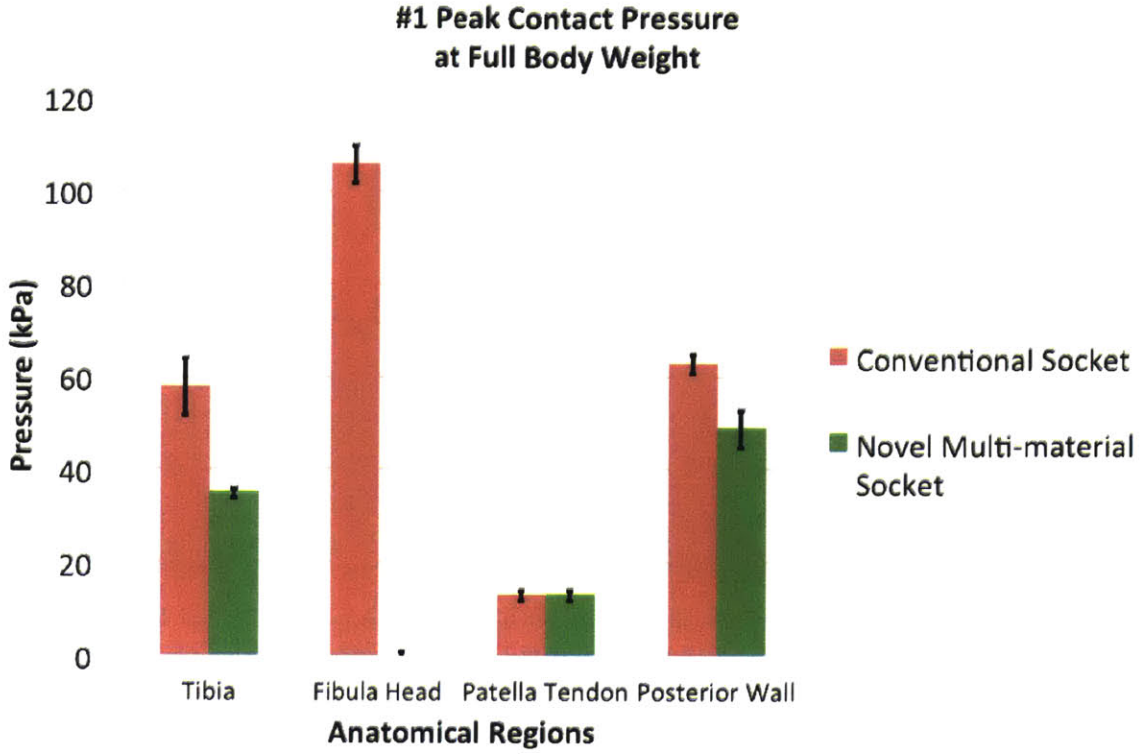

Figure 23: Peak contact pressures measure with standard deviation within F-Socket system for residuum #1.

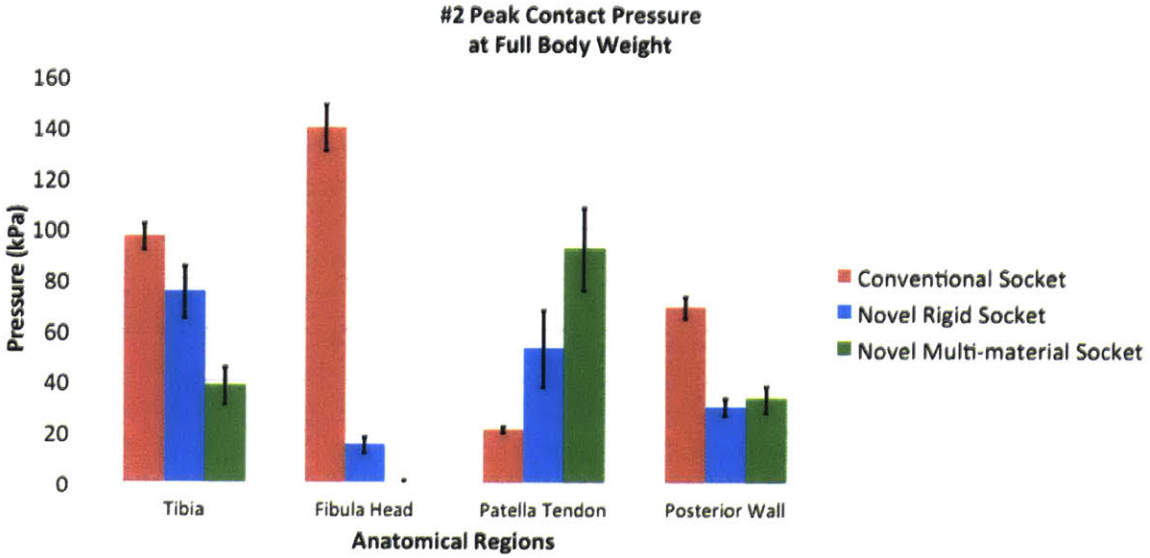

Figure 24: Peak contact pressures measure with standard deviation within F-Socket system for residuum #2

In residuum #2, the peak pressure values on the tibia region in the conventional socket were reduced by -23% and -61%; peak pressure on the fibula head was reduced by -89% and -100%; and peak pressures in the posterior wall region were reduced by -56% and -52% in the rigid and multi-material sockets respectively. There was an increase in the peak pressure on the patellar tendon region by +152% and +338% in the rigid socket and the multi-material socket respectively when compared to the conventional socket system.

4.4.3. Qualitative assessment

The patient was asked to give a qualitative assessment of 'fit' and 'comfort' in the novel prosthetic sockets as part of the evaluation. The rigid novel socket was structurally similar to his conventional socket. The rigid novel socket was 3-D printed with the Verowhite™ material, which is the most rigid option available. Without doubt, the patient concluded that the rigid novel socket felt "more comfortable" than both the conventional and the multi-material socket for full body weight loading. Both of the novel sockets were preferred in fit to the conventional socket. The patient noted that it would unthinkable to use a thin liner (3mm) with their conventional socket as used in the novel sockets. Furthermore, the patient noted that this is the first ever socket designed where it felt comfortable on the "first try."

4.5. DISCUSSION

Prosthetic socket design has evolved with advancement in technology through integrated CAD/CAM methodologies, FEA design frameworks and investigations of novel acquisition of data. In designs that showed reductions in residuum contact pressure at critical regions including those by Faustini *et al.* (2005) (82) and Sengeh and Herr (2013) (74), the shape of the evaluated socket was either provided by a prosthetist or it was not a final socket shape for practical use. Where quantitative biomechanical data input were used to simulate socket design in FEA, the models were not patient-specific and the soft tissue was assumed as a linear elastic material (9)(77) contrary to experimental data. Conclusions from a more recent review paper by Pirouzi *et al.* (2014) cement the already known theory that the clinical application of new socket designs were limited (15).

In this pilot study, our objectives were twofold. Firstly, we wanted to clinically investigate the fit of a prosthetic socket interface designed for a transtibial amputee through an automated, repeatable and quantitative methodology. We used a patient-specific biomechanical residuum model, validated mechanical properties of the liner and socket materials, and FEA to design and manufacture a custom liner and two novel 3-D printed prosthetic sockets for evaluation. Secondly, we argued that in comparison to a conventional socket system, the peak contact pressure in the novel socket designs would be lower on critical bony regions like the fibular head and tibia. Both the equilibrium shape of the novel sockets and the spatial material property at each surface element area were quantitatively derived using a patient-

specific "deformability map." The design-driving pressure field was altered at the patellar tendon and distal regions of the residuum. Furthermore, the material properties around the fibular head and distal region were altered to be the softest available material whereas those at the patellar tendon region were chosen to be the most rigid.

The approach used in this study allowed for the systematic evaluation of socket types, including those similar to standard PTB and TSB sockets using a validated residuum model. In this pilot, the novel sockets had peak pressures concentrated at the patellar tendon region. This allowed for a reduction in contact pressures at the distal tibia and the fibular head regions. At the distal tibia region and the fibular head region, the softest 3-D printable material (TangoBlack+™) was used for the multi-material socket. All these changes allowed for lower pressures at critical regions (fibular head and distal tibia) even at large forces like those experienced in running and high impact activities.

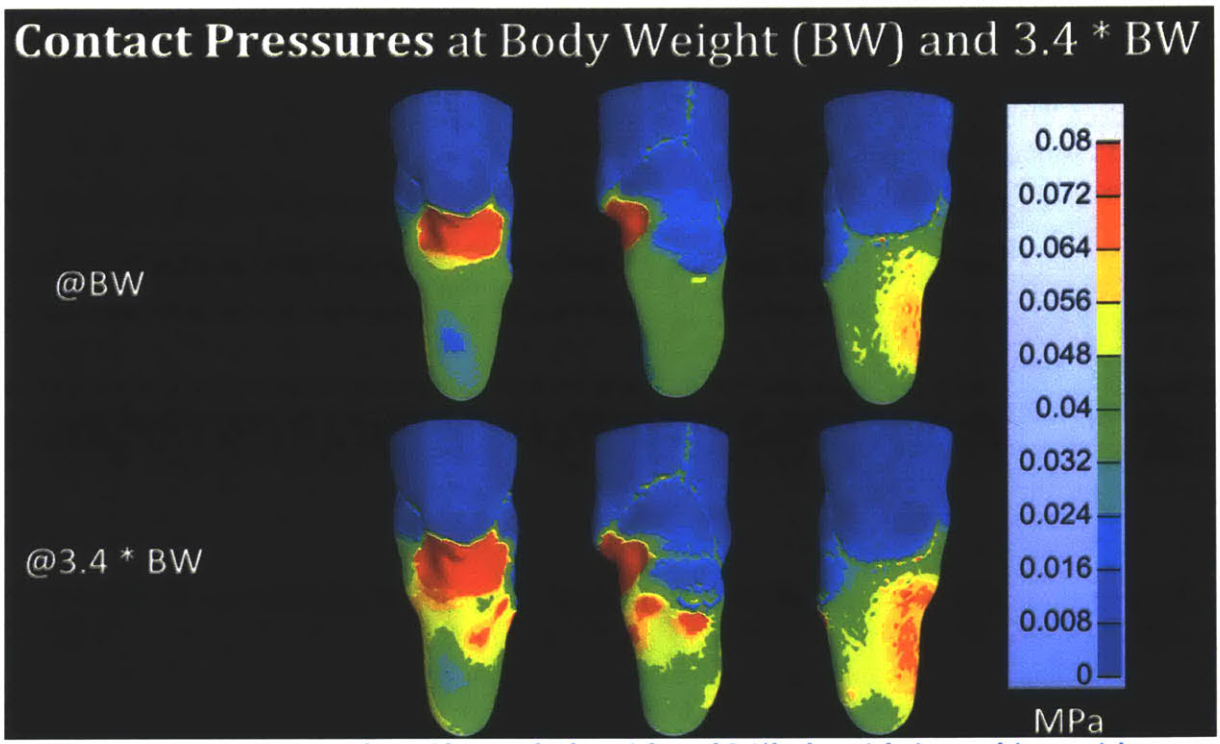

Figure 25: Contact pressure on the residuum at body weight and 3.4*body weight in a multi-material prosthetic socket with a soft distal region

In Figure 25, a multi-material socket model is evaluated at body weight (78 kg) and 3.4 times body weight. Even at these higher loads, the distal pressures are still under 50 kPa. These design features are critical for comfortable prosthetic sockets. As demonstrated by Portnoy *et al.* (2008), large distal pressures lead to increased internal strains in the muscle under the tibia and ultimately deep tissue injury (8). The patellar tendon region pressures in conventional socket designs in literature are usually very large (>100 kPa) (83). The way to achieve these reduced

pressures at critical regions is to design a prosthetic socket whose shape and mechanical property enhance loading at the patellar tendon.

While it is understood that reduced pressures and internal tissue strains and stress are desirable around bony protrusions for a comfortable prosthetic socket, there is still more to be learned about the overall pressure distributions on the residuum and their effect for a comfortable interface. Furthermore, an understanding of what tolerable pressure ranges at the patellar tendon are, for example, will lead to more optimized prosthetic sockets. From Table 9, for half-body weight standing (standing with two limbs) on residuum #1, there is a sharp increase in pressure values at the patellar tendon of the multi-material socket in comparison to conventional socket of +600%. However, for full body weight standing in the novel multi-material socket, there are reductions in pressure in the measured regions and no change on the patellar tendon bar. This means that peak pressures in other regions of the socket went up. A way to monitor where those increased pressures concentrate would be to more accurately map the pressure measuring sensors to the entire residuum beyond the few areas of interest studied here.

Residuum #1	% peak pressure change between conventional socket system and a multi-material novel socket	
Region	**Half Body Weight**	**Full Body Weight**
Tibia	+50	-40
Fibula Head	-92	-100
Patellar Tendon	+600	0
Posterior Wall	+19	-22

Table 9: % peak pressure change ((pressure conventional - pressure novel socket)/pressure conventional)*100 between the conventional socket and the multi-material socket on residuum #1

For residuum #2, the conventional socket is compared to both a novel multi-material socket and a novel rigid socket. As expected, there are very large pressure increases on the patella tendon region during loading between the novel socket designs and the conventional socket (see Table 10 and Table 11). However, there are also large reductions of pressure at the tibia, fibula head and posterior wall regions. These pressure decreases around the bony areas in the novel socket designs are significant and are probably reasons for why the patient reported feeling more comfortable in the novel sockets.

Residuum #2	% peak pressure change between conventional socket system and a multi-material novel socket	
Region	**Half Body Weight**	**Full Body Weight**
Tibia	-39	-61
Fibula Head	-74	-100
Patella Tendon	+217	+338

Posterior Wall	-45	-52

Table 10: % peak pressure change in residuum #2 between the conventional socket and the multi-material novel socket

Residuum #2	% peak pressure change between conventional socket system and a rigid novel socket
Region	**Full Body Weight**
Tibia	-22
Fibula Head	-89
Patella Tendon	+152
Posterior Wall	-57

Table 11: % peak pressure change in residuum #2 between the conventional socket and the rigid novel socket

There is more to be learned from evaluating the models particularly related to internal soft tissue strains and stresses which lead to soft tissue injuries under load (84). The maximum shear Lagrange strains seen in Figure 26 are comparable for the rigid design and the novel socket design for body weight load especially under the tibia and fibular bones.

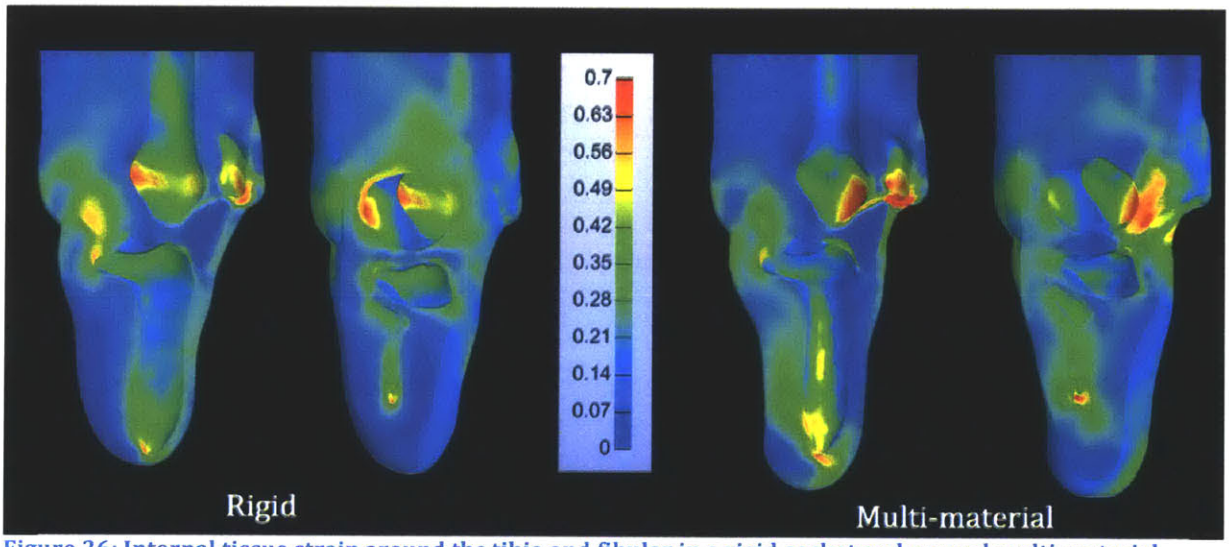

Figure 26: Internal tissue strain around the tibia and fibular in a rigid socket and a novel multi-material socket

4.5.1. Other Limitations

Currently, custom liner manufacturing as proposed here is both time-intensive and costly. To generate a liner, a multipart mold must be created to pour the uniform thickness silicone liner. For this study, only a positive mold was 3-D printed and the silicone was manually poured over it to create the liner. In the future, a more accurate approach should be used to guarantee that the liner

thickness matches the model. Future modeling approaches will also integrate conventional liners of uniform thickness to address these issues.

In this current novel multi-material socket design, we are not fully testing the effects of a continuously spatially varying socket. The five materials selected for the socket design from the displaceability map and the set of printable materials available really just give two categories: rigid and soft. To increase the spread of materials available for selection in manufacturing, we will investigate the use of bitmap 3-D printing, which is an option on the current Polyjet 3-D printing technology. Material studies will be done to properly model the behavior of all the new material options to fully study the effect of spatially varying mechanical properties on a residuum.

While the novel socket design framework used in this study through FEA yielded a better fit for full body weight loading through qualitative and quantitative evaluations in comparison to a conventional socket designed by a trained prosthetist, the approach may still be improved for immediate clinical use. In the donning step for example, sliding with friction versus the current tied contact between the liner surface and the socket could be investigated. Furthermore, loading mechanisms (currently an upward Z displacement of the socket relative to a fixed top surface) must be further investigated including the ability of the bones to move in the medial-lateral direction as observed by Papaioannou *et al.* (2010). An integral component missing in this framework is input from patients. Evidently, there are physical sensations that cannot be fully captured using just an imaging dataset. Other information, such as location of scar tissue and sensitive regions, have not yet been integrated into our approach. However, there is a capability to do so in the future by identifying specific regions where one could deviate from the quantitative design framework as already done with the design pressure field for example.

4.5.2. Future work

The designs evaluated in this study were automated but the solutions were not optimized. For future work, a set of optimizations that seek to minimize the contact pressure at bony areas and the corresponding internal soft tissue strains will be investigated. The pressure field used to drive the equilibrium shape of the socket was a linear mapping between the minimum and maximum pressures provided. Although the applied pressures were comparable to pressure data ranges in previous literature, it would be transformational to link design-driving pressure fields to comfortable interface pressures for a prosthetic socket on a patient. The design rules that govern the displaceability map, the linear function between the map and the applied pressure, the linear function between the map and the socket material impedance, the socket cutline, and other features all need to be further studied and optimized. The design should ultimately be evaluated for level ground walking and running if the solutions would be clinically applicable. Longitudinal studies where patients evaluate the socket over an extended period of time should also be carried out. A major factor for socket discomfort is related to volume change in the residuum. More work that investigates how such a volume change affects the

design solutions will be useful. Since the methodology in this study is repeatable, it is feasible to take regular MRI datasets over an extended period of time to investigate various socket designs for a given patient.

4.6. CONCLUSION

Current advances in the design and evaluation of prosthetic sockets have not achieved the desirable outcome of an automated design and manufacturing process for comfortable prosthetic sockets. This is in part because there are too many unknown variables that affect socket fit and ultimately comfort, including interface contact pressure, internal soft tissue strains and stresses, liner and suspension types. Furthermore, for all these variables, the patient-specific ranges within which they should be optimized are also unknown. This paper presents the first fully automated, quantitative and patient-specific rigid and multi-material socket design (shape and spatial mechanical properties) based on a predictive biomechanical model. The initial results from this pilot study are encouraging, showing reduced interface pressure measurements on critical bony regions in the novel sockets in comparison to a conventional socket system. With increased computational power for design optimization, cheaper tools for patient-specific model identification, faster and cheaper computer-aided manufacturing, CAD sockets will soon be readily used in clinics.

4.7. ACKNOWLEDGEMENTS

This work was funded resources provided by the Robert Wood Johnson Foundation and the MIT Media Lab Consortium.

5. Chapter 5: Conclusion

This thesis presents a methodology for the quantitative design of transtibial prosthetic sockets (both equilibrium shape derivation and spatial variation of multi-material properties) through an automated and repeatable process that reduces interface pressure at bony regions of the residuum during loading. To accomplish this objective requires a multi-disciplinary approach that involves medical imaging, soft tissue modeling, and advanced CAD/CAM processes (see Figure 27). Furthermore, the dataset must be continuous through the entire pipeline, such that there is point correspondence from the residuum anatomy to the design files that are used for the manufactured object. Today, a combination of MRI, custom indentors, modeling software and Polyjet multi-material 3-D printing makes this possible.

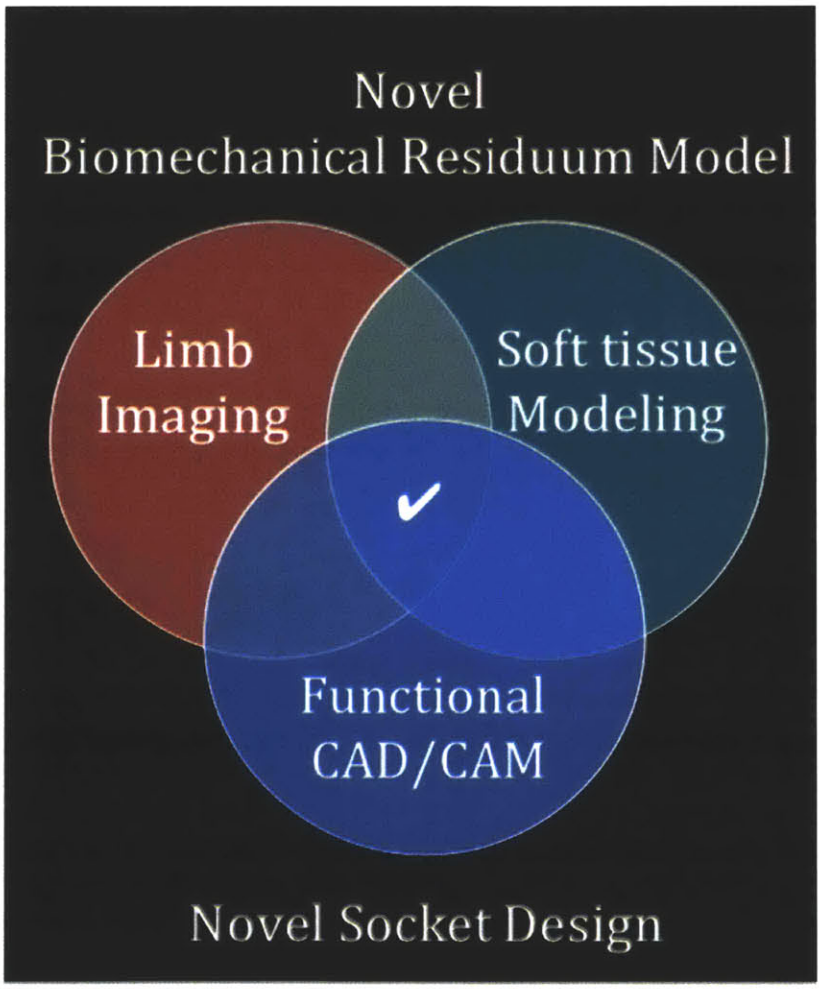

Figure 27: Socket design at the intersection of various fields

5.1. Thesis Contributions

This thesis work has been central to the advances made towards the broader objective of the Biomechatronics Group to design novel mechanical interfaces for the human anatomy. More specifically, I developed the research methodology to acquire MRI data with markers for residual limbs across multiple patients. Using the open source toolbox GIBBON Code, I segmented those MRI data for model development. As demonstrated from results summarized in Study I and Study II, I developed iFEA optimization methodologies based on GIBBON and FEBio using experimental data acquired by my collaborators to identify patient-specific biomechanical material constants for N= 6 patients. Finally, Study III evaluated the result of two novel sockets designed using such a predictive biomechanical model and a design framework co-developed with Kevin Moerman. This thesis work led to several peer-reviewed manuscripts for which I am the lead author on three.

5.2. Outlook

Computational socket design as a field will grow in leaps and bounds over the next couple of years. There exists a future where patients all around the world will have their residuum limbs scanned by low-cost digital imaging devices with sufficient patient-specific information to inform predictive biomechanical models. Such models will be input into computational frameworks, which will recommend a perfectly automated interface with a shape and spatial mechanical property that is optimized for comfort. In such a future, the patient will have their sockets manufactured and functionally ready for use quickly and cheaply. In the recent past, this vision would have been baseless but undoubtedly, such processes will become conventional for most mechanical interfaces for the human body. That is exciting!

List of Figures

List of Tables

REFERENCES

1. Ziegler-Graham K, MacKenzie EJ, Ephraim PL, Travison TG, Brookmeyer R. Estimating the prevalence of limb loss in the United States: 2005 to 2050. Arch Phys Med Rehabil [Internet]. Elsevier; 2008;89(3):422–9. Available from: http://www.ncbi.nlm.nih.gov/pubmed/18295618
2. Dillingham TR, Pezzin LE, MacKenzie EJ. Limb amputation and limb deficiency: epidemiology and recent trends in the United States. South Med J. 2002;95(8):875–83.
3. Sanders JE, Rogers EL, Sorenson E a., Lee GS, C., Abrahamson D. CAD/CAM transtibial prosthetic sockets from central fabrication facilities: How accurate are they? J Rehabil Res Dev [Internet]. 2007 [cited 2011 Dec 7];44(3):395–406. Available from: http://www.rehab.research.va.gov/jour/07/44/3/pdf/sanders.pdf
4. Sanders JE, Severance MR, Allyn KJ. Computer-socket manufacturing error: how much before it is clinically apparent? J Rehabil Res Dev [Internet]. 2012 Jan;49(4):567–82. Available from: http://www.ncbi.nlm.nih.gov/pubmed/22773260
5. Meulenbelt HEJ, Dijkstra PU, Jonkman MF, Geertzen JHB. Skin problems in lower limb amputees: a systematic review. Disabil Rehabil. Informa UK Ltd UK; 2006 May;28(10):603–8.
6. Portnoy S, Siev-Ner I, Shabshin N, Gefen a. Effects of sitting postures on risks for deep tissue injury in the residuum of a transtibial prosthetic-user: a biomechanical case study. Comput Methods Biomech Biomed Engin [Internet]. 2011;14:1009–19. Available from: http://www.ncbi.nlm.nih.gov/pubmed/20694863
7. Silver-Thorn MB, Steege JW, Childress DS. A review of prosthetic interface stress investigations. J Rehabil Res Dev [Internet]. 1996 Jul;33(3):253–66. Available from: http://www.ncbi.nlm.nih.gov/pubmed/8823673
8. Portnoy S, Yizhar Z, Shabshin N, Itzchak Y, Kristal a, Dotan-Marom Y, et al. Internal mechanical conditions in the soft tissues of a residual limb of a trans-tibial amputee. J Biomech [Internet]. 2008 Jan [cited 2013 Mar 19];41(9):1897–909. Available from: http://www.ncbi.nlm.nih.gov/pubmed/18495134
9. Lee WCC, Zhang M. Using computational simulation to aid in the prediction of socket fit: A preliminary study. Med Eng Phys. 2007;29(8):923–9.
10. McGarry A, McHugh B, Duers J, Buis AWP. Design of manikin for testing of residual-limb shape-capture method: technical note. J Rehabil Res Dev. 2011;48(3):245–51.
11. Gerschutz MJ, Haynes ML, Nixon DM, Colvin JM. Tensile strength and impact resistance properties of materials used in prosthetic check sockets, copolymer sockets, and definitive laminated sockets. J Rehabil Res Dev [Internet]. 2011 [cited 2013 Apr 25];48(8):987–1004. Available from: http://www.rehab.research.va.gov/jour/11/488/pdf/gershutz488.pdf
12. Buis AWP, Condon B, Brennan D, McHugh B, Hadley D. Magnetic resonance imaging technology in transtibial socket research: A pilot study. J Rehabil Res Dev [Internet]. 2006 [cited 2012 Jan 12];43(7):883–90. Available from: http://www.rehab.research.va.gov/jour/06/43/7/pdf/buis.pdf
13. Zheng Y, Mak AF, Lue B. Objective assessment of limb tissue elasticity: development of a manual indentation procedure. J Rehabil Res Dev [Internet]. 1999 Apr;36(2):71–85. Available from: http://www.ncbi.nlm.nih.gov/pubmed/10661523
14. Tönük E, Silver-Thorn MB. Nonlinear elastic material property estimation of lower extremity residual limb tissues. IEEE Trans Neural Syst Rehabil Eng. 2003;11(1):43–53.
15. Pirouzi G, Osman N a A, Eshraghi A, Ali S, Gholizadeh H, Abas W a BW. Review of the Socket Design and Interface Pressure Measurement for Transtibial Prosthesis. Sci World J [Internet]. 2014;2014:9. Available from: http://dx.doi.org/10.1155/2014/849073
16. Mak AF, Zhang M, Boone DA. State-of-the-art research in lower-limb prosthetic biomechanics-socket interface: a review. J Rehabil Res Dev [Internet]. 2001;38(2):161–74. Available from: http://www.ncbi.nlm.nih.gov/pubmed/11392649
17. Portnoy S, Siev-Ner I, Shabshin N, Kristal a., Yizhar Z, Gefen a. Patient-specific analyses of deep tissue loads post transtibial amputation in residual limbs of multiple prosthetic users. J Biomech. 2009;42(16):2686–93.
18. Papaioannou G, Mitrogiannis C, Nianios G, Fiedler G. Assessment of amputee socket-stump-residual bone kinematics during strenuous activities using Dynamic Roentgen Stereogrammetric Analysis. J Biomech [Internet]. 2010 Mar 22 [cited 2012 Jan 13];43(5):871–8. Available from: http://www.ncbi.nlm.nih.gov/pubmed/20047746
19. Bosboom EMH, Hesselink MKC, Oomens CWJ, Bouten CVC, Drost MR, Baaijens FPT. Passive transverse mechanical properties of skeletal muscle under in vivo compression. J Biomech. 2001;34:1365–8.
20. Van Loocke M, Lyons CG, Simms CK. A validated model of passive muscle in compression. J Biomech. 2006;39:2999–3009.

21. Van Loocke M, Lyons CG, Simms CK. Viscoelastic properties of passive skeletal muscle in compression: Stress-relaxation behaviour and constitutive modelling. J Biomech. 2008;41:1555–66.

22. Palevski A, Glaich I, Portnoy S, Linder-Ganz E, Gefen A. Stress relaxation of porcine gluteus muscle subjected to sudden transverse deformation as related to pressure sore modeling. J Biomech Eng. 2006;128:782–7.

23. Groves RB, Coulman S a, Birchall JC, Evans SL. Quantifying the mechanical properties of human skin to optimise future microneedle device design. Comput Methods Biomech Biomed Engin. 2012 Jan;15(1):73–82.

24. Tran H V, Charleux F, Rachik M, Ehrlacher a, Ho Ba Tho MC. In vivo characterization of the mechanical properties of human skin derived from MRI and indentation techniques. Comput Methods Biomech Biomed Engin. 2007 Dec;10(6):401–7.

25. Dubuis L, Avril S, Debayle J, Badel P. Identification of the material parameters of soft tissues in the compressed leg. Comput Methods Biomech Biomed Engin. 2011;15(November):3–11.

26. Vannah WM, Childress DS. Indentor tests and finite element modeling of bulk muscular tissue in vivo. J Rehabil Res Dev. 1996;33(3):239–52.

27. Portnoy S, Siev-Ner I, Yizhar Z, Kristal A, Shabshin N, Gefen A. Surgical and morphological factors that affect internal mechanical loads in soft tissues of the transtibial residuum. Ann Biomed Eng. 2009;37:2583–605.

28. Goh J, Lee P, Toh S, Ooi C. Development of an integrated CAD-FEA process for below-knee prosthetic sockets. Clin Biomech [Internet]. 2005 [cited 2013 Apr 25];20(6):623–9. Available from: http://www.sciencedirect.com/science/article/pii/S026800330500029X

29. Zheng YP, Mak a F, Leung a K. State-of-the-art methods for geometric and biomechanical assessments of residual limbs: a review. J Rehabil Res Dev. 2001;38:487–504.

30. Hendriks FM, Brokken D, van Eemeren JTWM, Oomens CWJ, Baaijens FPT, Horsten JB a M. A numerical-experimental method to characterize the non-linear mechanical behaviour of human skin. Skin Res Technol. 2003;9(3):274–83.

31. Moerman KM. GIBBON (Hylobates Agilis). 2014.

32. Moerman KM, Nederveen AJ, Simms CK. IMAGE BASED MODEL CONSTRUCTION , BOUNDARY CONDITION SPECIFICATION AND INVERSE FEA CONTROL : A BASIC MATLAB TOOLKIT FOR FEBIO. 2013;7–8.

33. Maas S a, Ellis BJ, Ateshian G a, Weiss J a. FEBio: finite elements for biomechanics. J Biomech Eng [Internet]. 2012 Jan [cited 2014 Aug 9];134(1):011005. Available from: http://www.pubmedcentral.nih.gov/articlerender.fcgi?artid=3705975&tool=pmcentrez&rendertype=abstract

34. Robson, Matthew, Gatehouse, Peter, Bydder, Mark, Bydder G. Magnetic Resonance: An Introduction to Ultrashort TE (UTE) Imaging. Journal of Computer Assisted Tomography. 2003. p. 825–46.

35. Herr HM, Petron A. Physiological measurement device or wearable device interface simulator and method of use [Internet]. USA; 2013. Available from: https://www.google.com/patents/US20130197318

36. Josse G, George J, Black D. Automatic measurement of epidermal thickness from optical coherence tomography images using a new algorithm. Ski Res Technol. Blackwell Publishing Ltd; 2011 Mar;17(3):314–9.

37. Mogensen M, Morsy HA, Thrane L, Jemec GBE. Morphology and Epidermal Thickness of Normal Skin Imaged by Optical Coherence Tomography. Dermatology. 2008;217(1):14–20.

38. Moore TL, Lunt M, McManus B, Anderson ME, Herrick AL. Seventeen-point dermal ultrasound scoring system—a reliable measure of skin thickness in patients with systemic sclerosis. Rheumatology. 2003;42(12):1559–63.

39. Si H. TetGen, a Delaunay-Based Quality Tetrahedral Mesh Generator. ACM Trans Math Softw. ACM; 2015 Feb;41(2):1–36.

40. Laursen TA, Maker BN. An augmented Lagrangian quasi-Newton solver for constrained nonlinear finite element applications. Int J Numer Methods Eng. 1995 Nov;38(21):3571–90.

41. Laursen TA, Simo JC. A continuum-based finite element formulation for the implicit solution of multibody, large deformation-frictional contact problems. Int J Numer Methods Eng. 1993 Oct;36(20):3451–85.

42. Laursen TA. Computational Contact and Impact Mechanics: Fundamentals of Modeling Interfacial Phenomena in Nonlinear Finite Element Analysis (Google eBook). Berlin: Springer; 2002.

43. Ateshian GA, Maas S, Weiss JA. Finite element algorithm for frictionless contact of porous permeable media under finite deformation and sliding. J Biomech Eng. 2010 Jun;132(6):061006.

44. Itskov M. Tensor Algebra and Tensor Analysis for Engineers. 2nd ed. Springer; 2009.

45. Bonet J, Wood RDD. Nonlinear Continuum Mechanics for Finite Element Analysis. Cambridge University Press; 2008.

46. Holzapfel GA. Nonlinear Solid Mechanics, A continuum approach for engineering. John Wiley & Sons Ltd.; 2004.

47. Fung YC. Biomechanics, Mechanical Properties of Living Tissues. New York: Springer-Verlag New York Inc.; 1993.

48. Puso MA, Weiss JA. Finite Element Implementation Viscoelasticity Using a Discrete Spectrum Approximation. 1998;120(February).

49. Levenberg K. A Method for the Solution of Certain Problems in Least Square. Q J Appl Math. 1944;2:164–8.

50. Bensamoun SF, Ringleb SI, Littrell L, Chen Q, Brennan M, Ehman RL, et al. Determination of thigh muscle stiffness using magnetic resonance elastography. J Magn Reson Imaging. 2006;23(2):242–7.

51. Frauziols F, Molimard J, Navarro L, Badel P, Viallon M, Testa R, et al. Prediction of the biomechanical effects of compression therapy by finite element modeling and ultrasound elastography. IEEE Trans Biomed Eng. 2015;62(4):1011–9.

52. Lim J, Hong J, Chen WW, Weerasooriya T. Mechanical response of pig skin under dynamic tensile loading. Int J Impact Eng. 2011;38:130–5.

53. Mukherjee S, Chawla a., Karthikeyan B, Soni a. Finite element crash simulations of the human body: Passive and active muscle modelling. Sadhana - Acad Proc Eng Sci. 2007;32(August):409–26.

54. Portnoy S, Yarnitzky G, Yizhar Z, Kristal A, Oppenheim U, Siev-Ner I, et al. Real-time patient-specific finite element analysis of internal stresses in the soft tissues of a residual limb: a new tool for prosthetic fitting. Ann Biomed Eng. Kluwer Academic Publishers-Plenum Publishers; 2007 Jan;35(1):120–35.

55. Moerman KM, Holt C a., Evans SL, Simms CK. Digital image correlation and finite element modelling as a method to determine mechanical properties of human soft tissue in vivo. J Biomech. 2009;42:1150–3.

56. Moerman KM, Sprengers AMJ, Nederveen AJ, Simms CK. A novel MRI compatible soft tissue indentor and fibre Bragg grating force sensor. Med Eng Phys. 2013;35:486–99.

57. Moerman KM, Sprengers AM, Simms CK, Lamerichs RM, Stoker J, Nederveen AJ. Validation of SPAMM tagged MRI based measurement of 3D soft tissue deformation. Med Phys. 2011;38(3):13.

58. Moerman KM, Sprengers AMJ, Simms CK, Lamerichs RM, Stoker J, Nederveen AJ. Validation of Continuously Tagged MRI for the Measurement of Dynamic 3D Soft Tissue Deformation. Med Phys. 2012 Apr;39(4):1793–810.

59. Froeling M, Nederveen AJ, Heijtel DFR, Lataster A, Bos C, Nicolay K, et al. Diffusion-tensor MRI reveals the complex muscle architecture of the human forearm. J Magn Reson Imaging. Wiley Subscription Services, Inc., A Wiley Company; 2012;n/a – n/a.

60. Pirouzi G, Osman N a A, Eshraghi a, Ali S, Gholizadeh H, Abas W a BW. Review of the Socket Design and Interface Pressure Measurement for Transtibial Prosthesis. Sci J [Internet]. 2014;2014:9. Available from: http://dx.doi.org/10.1155/2014/849073

61. Zhang M, Mak AF, Roberts VC. Finite element modelling of a residual lower-limb in a prosthetic socket: a survey of the development in the first decade. Med Eng Phys [Internet]. 1998;20(5):360–73. Available from: http://www.ncbi.nlm.nih.gov/pubmed/9773689

62. Zheng YP, Mak a F, Leung a K. State-of-the-art methods for geometric and biomechanical assessments of residual limbs: a review. J Rehabil Res Dev [Internet]. 2001;38(5):487–504. Available from: http://www.ncbi.nlm.nih.gov/pubmed/11732827

63. Glaser KJ, Manduca A, Ehman RL. Review of MR elastography applications and recent developments. J Magn Reson Imaging [Internet]. 2012 Oct [cited 2013 Mar 1];36(4):757–74. Available from: http://www.ncbi.nlm.nih.gov/pubmed/22987755

64. Greenleaf JF, Fatemi M, Insana M. Selected methods for imaging elastic properties of biological tissues. Annu Rev Biomed Eng [Internet]. 2003 Jan [cited 2012 Nov 2];5:57–78. Available from: http://www.ncbi.nlm.nih.gov/pubmed/12704084

65. Moerman KM, Simms CK, Nagel T. Control of Tension-Compression Asymmetry in Ogden Hyperelasticity with Application to Soft Tissue Modelling. J Mech Behav Biomed Mater. In press.

66. Sengeh DM, Moerman KM, Petron A, Herr HM. Multi-Material 3-D Viscoelastic Model of a Transtibial Residuum from In-vivo Indentation and MRI Data. J Mech Behav Biomed Mater.

67. Zheng Y, Mak a. FT. Effective elastic properties for lower limb soft tissues from manual indentation experiment. IEEE Trans Rehabil Eng. 1999;7(3):257–67.

68. Muller M, P TBSEDC. Total Surface Bearing Trans-Tibial Socket Design Impression Techniques.

69. Smith DG, Burgess EM. The use of CAD/CAM technology in prosthetics and orthotics--current clinical models and a view to the future. J Rehabil Res Dev [Internet]. 2001;38(3):327–34. Available from: http://www.ncbi.nlm.nih.gov/pubmed/11440264

70. Herbert N, Simpson D, Spence WD, Ion W. A preliminary investigation into the development of 3-D printing of prosthetic sockets. J Rehabil Res Dev [Internet]. 2005 [cited 2012 Oct 26];42(2):141. Available from: http://www.rehab.research.va.gov/jour/05/42/2/herbert.html

71. Jin Y, Plott J, Chen R, Wensman J, Shih A. Additive Manufacturing of Custom Orthoses and Prostheses – A Review. Procedia CIRP [Internet]. Elsevier B.V.; 2015;36:199–204. Available from: http://linkinghub.elsevier.com/retrieve/pii/S2212827115004370

72. Dumbleton T, Buis AWP, McFadyen A, McHugh BF, McKay G, Murray KD, et al. Dynamic interface pressure

distributions of two transtibial prosthetic socket concepts. J Rehabil Res Dev [Internet]. 2009 Jan [cited 2014 Sep 29];46(3):405–15. Available from: http://www.ncbi.nlm.nih.gov/pubmed/19675992

73. Rogers B, Bosker GW, Crawford RH, Faustini MC, Neptune RR, Walden G, et al. Advanced trans-tibial socket fabrication using selective laser sintering. Prosthet Orthot Int [Internet]. SAGE Publications; 2007 [cited 2012 Jan 13];31(1):88. Available from: http://poi.sagepub.com/content/31/1/88.short

74. Sengeh DM, Herr H. A Variable-Impedance Prosthetic Socket for a Transtibial Amputee Designed from Magnetic Resonance Imaging Data. JPO J Prosthetics Orthot [Internet]. 2013 Jul;25(3):129–37. Available from: http://content.wkhealth.com/linkback/openurl?sid=WKPTLP:landingpage&an=00008526-201307000-00006

75. Facoetti G, Gabbiadini S, Colombo G, Rizzi C. Knowledge-based System for Guided Modeling of Sockets for Lower Limb Prostheses. Comput Des. 2010;7(5):723–37.

76. Papaioannou G, Tsiokos D, Fiedler G, Mitrogiannis C, Avdeev I, Wood J, et al. Dynamic Radiography Imaging as a Tool in the Design and Validation of a Novel Intelligent Amputee Socket. In: Tavares JMRS, Jorge RMN, editors. Computational Vision and Medical Image Processing: Recent Trends, [Internet]. Dordrecht: Springer Netherlands; 2011 [cited 2012 Nov 4]. p. 91–112. Available from: http://www.springerlink.com/index/10.1007/978-94-007-0011-6

77. Wu C, Chang C, Hsu A, Lin C, Chen S, Chang G. A proposal for the pre-evaluation protocol of below-knee socket design - Integration pain tolerance with finite element analysis. J Chinese Inst Eng [Internet]. 2003 [cited 2013 Apr 25];26(6):853–60. Available from: http://www.tandfonline.com/doi/full/10.1080/02533839.2003.9670840

78. Colombo G, Facoetti G, Rizzi C, Vitali A, Zanello A. Automatic 3D Reconstruction of Transfemoral Residual Limb from MRI Images. In: Duffy V, editor. Digital Human Modeling and Applications in Health, Safety, Ergonomics, and Risk Management Human Body Modeling and Ergonomics SE - 38. Springer Berlin Heidelberg; 2013. p. 324–32.

79. Öberg T, Lilja M, Johansson T, Karsznia A. Clinical evaluation of trans-tibial prosthesis sockets: a comparison between CAD CAM and conventionally produced sockets. Prosthet Orthot Int [Internet]. SAGE Publications; 1993 [cited 2012 Jan 13];17(3):164. Available from: http://poi.sagepub.com/content/17/3/164.short

80. Johnson GA, Tramaglini DM, Levine RE, Ohno K, Choi NY, Woo SLY. Tensile and viscoelastic properties of human patellar tendon. J Orthop Res. 1994;12(6):796–803.

81. Ateshian GA, Ricken T. Multigenerational interstitial growth of biological tissues. Biomech Model Mechanobiol. 2010 Dec;9(6):689–702.

82. Faustini MC, Crawford RH, Neptune RR, Rogers WE, Bosker G. Design and Analysis of Orthogonally Compliant Features for Local Contact Pressure Relief in Transtibial Prostheses. J Biomech Eng [Internet]. 2005 [cited 2011 Dec 7];127(6):946. Available from: http://link.aip.org/link/JBENDY/v127/i6/p946/s1&Agg=doi

83. Convery P, Buis a W. Conventional patellar-tendon-bearing (PTB) socket/stump interface dynamic pressure distributions recorded during the prosthetic stance phase of gait of a trans-tibial amputee. Prosthet Orthot Int. 1998;22:193–8.

84. Oomens CWJ, Loerakker S, Bader DL. The importance of internal strain as opposed to interface pressure in the prevention of pressure related deep tissue injury. J Tissue Viability. 2010 May;19(2):35–42.